**An Experiment To Measure The Electromagnetic Form-factors Of The Neutron In The Timelike Region At Adone.**

(Article begins on next page)

15 December 2021

# INFN - Laboratori Nazionali di Frascati

**LNF-87/18(R)**

17 Aprile 1987

*FENICE COLLABORATION*

A. Antonelli, R. Baldini Ferroli, M. E. Biagini, V. Bidoli, T. Bressani, R. Calabrese, R. Cardarelli, R. Carlin, C. Cernigoi, S. Costa, L. Cugusi, B. Dainese, P. Dalpiaz, S. De Simone, G. De Zorzi, U. Dosselli, B. Dulach, P. Ferretti Dalpiaz, R. Giantin, S. Guiducci, F. Iazzi, E. Luppi, S. Marcello, A. Masoni, G. Milani, B. Minetti, M. Morandin, M. Nigro, L. Paoluzi, G. Pauli, F. Petrucci, G. Pitacco, M. Posocco, M. A. Preger, G. Puddu, L. Santi, R. Santonico, P. Sartori, M. Savrie`, M. Schioppa, S. Serci, M. Serio, M. Spinetti, L. Tecchio, V. Tricomi, C. Voci:

## AN EXPERIMENT TO MEASURE THE ELECTROMAGNETIC FORM FACTORS OF THE NEUTRON IN THE TIME-LIKE REGION AT ADONE

# AN EXPERIMENT TO MEASURE THE ELECTROMAGNETIC FORM FACTORS OF THE NEUTRON IN THE TIME-LIKE REGION AT ADONE

*FENICE COLLABORATION*

A. Antonelli[3], R. Baldini Ferroli[3], M. E. Biagini[3], V. Bidoli[5], T. Bressani[6], R. Calabrese[2], R. Cardarelli[5], R. Carlin[4], C. Cernigoi[7], S. Costa[6], L. Cugusi[1], B. Dainese[4], P. Dalpiaz[2], S. De Simone[3], G. De Zorzi[5], U. Dosselli[4], B. Dulach[3], P. Ferretti Dalpiaz[2], R. Giantin[4], S. Guiducci[3], F. Iazzi[6], E. Luppi[2], S. Marcello[1], A. Masoni[1], G. Milani[7], B. Minetti[6], M. Morandin[4], M. Nigro[4], L. Paoluzi[5], G. Pauli[7], F. Petrucci[2], G. Pitacco[4], M. Posocco[4], M. A. Preger[3], G. Puddu[1], L. Santi[7], R. Santonico[5], P. Sartori[4], M. Savrie'[2], M. Schioppa[3], S. Serci[1], M. Serio[3], M. Spinetti[3], L. Tecchio[6], V. Tricomi[6], C. Voci[4].

1. Cagliari University and Sezione INFN
2. Ferrara University and Sezione INFN
3. INFN National Laboratory, Frascati
4. Padova University and Sezione INFN
5. Rome Universities and Sezione INFN
6. Torino University and Sezione INFN
7. Trieste University and Sezione INFN

## TABLE OF CONTENTS

We present a physics program that will be run starting in 1987 at the Adone machine in Frascati, when it will come back to $e^+e^-$ operation. The main item is the measurement of the neutron electromagnetic form factors in the time-like region via the reaction $e^+e^- \to \bar{n}n$; other channels are under consideration for new measurements or monitoring purposes. The machine developments related to the $e^+e^-$ operation are discussed and the detection apparatus, presently under construction, is described.

## 9-1. The nucleon e.m.f.f. in the time-like region.

The experimental knowledge of the e.m.f.f. of the nucleon is only partially satisfactory. Regarding the proton there are many precise measurements in the space-like region (ep elastic scattering at $q^2 \geq 0$) and the $q^2$ behaviour is fairly established; a high statistics measurement in the time-like region is under way at LEAR (exp. PS170, $\bar{p}p \to e^+e^-$). The situation is more sombre for the neutron: at $q^2 \geq 0$ data are extracted from electron-deuteron scattering and the procedure can lead to systematic errors; moreover the neutron electric form factor is quite small, vanishing at $q^2=0$, and its measurement is affected by large statistical errors. In the time-like region there exists no determination of the neutron form factors.

The cross section in the space-like region is given by the well known Rosenbluth formula; in the time-like region it is written

$$\frac{d\sigma}{d\Omega} = \frac{\alpha^2\beta}{4s} \left[ |G_M|^2(1+\cos^2\theta) - \frac{4M^2}{q^2}|G_E|^2\text{sen}^2\theta \right] \tag{1.1}$$

for the $e^+e^-$ annihilation into nucleon-antinucleon [1]; M is the nucleon mass, $s=-q^2$ the squared c.m. energy, $\beta$ the nucleon velocity. The corresponding integrated cross section is

$$\sigma_I = \frac{4\pi\alpha^2\beta}{3s} \left[ |G_M|^2 - \frac{2M^2}{q^2}|G_E|^2 \right] \tag{1.2}$$

For the nucleon-antinucleon annihilation into $e^+e^-$ the formulae are[2]:

$$\left(\frac{d\sigma}{d\Omega}\right)_{CM} = \frac{\alpha^2}{4s\beta} \left[ |G_M|^2(1+\cos^2\theta) - \frac{4M^2}{q^2}|G_E|^2\sin^2\theta \right] \qquad (1.3)$$

$$\sigma_2 = \frac{4\pi\alpha^2}{3s\beta} \left[ |G_M|^2 - \frac{2M^2}{q^2}|G_E|^2 \right] \qquad (1.4$$

where $\beta$ is again the nucleon or antinucleon velocity.

The two cross sections are related by phase space factors; for instance

$$\sigma_1 = (p_{\bar{p}}/p_e)^2 \ \sigma_2 \qquad (1.5)$$

with $p_{\bar{p}}$ is the antinucleon momentum in the $e^+e^-$ annihilation and $p_e$ is the electron c.m. momentum in the nucleon-antinucleon annihilation.

We recall that the functions of $q^2$ $G_E$ and $G_M$ are the Sachs electric and magnetic form factors of the proton or neutron; they are real in the space-like region where the following conditions hold: at $q^2=0$ $G_{E,p}=1$, $G_{E,n}=0$, $G_{M,p}=2.79$, $G_{M,n}=-1.91$; p and n refer to proton and neutron. In the time-like region $G_E$ and $G_M$ become complex numbers, equal at $q^2=-4M^2$, i.e. at the threshold for the annihilation reaction.

The measured $q^2$ behaviour in the space-like region of $G_E$ and $G_M$ has been the object of many phenomenological fits. The most popular was the dipole fit that can be summarized by the formula $G_D=1/(1+q^2/0.71)^2$ and the assumptions $G_{M,n}/|\mu_n|=G_{M,p}/\mu_p=G_{E,p}=G_D$, $G_{E,n}=0$, where $\mu$ is the magnetic moment. Very precise measurements at $q^2\approx0$ and at high $q^2$ rule out this approximation; moreover in the time-like region $G_D$ is about one order of magnitude below the data.

Another approach is the vector meson dominance model (VDM): the connection between the hadron vertex and the electromagnetic vertex is supposed to happen according to fig. 1. $V_0$ is a vector meson, for instance $\rho,\omega,\varphi$; the
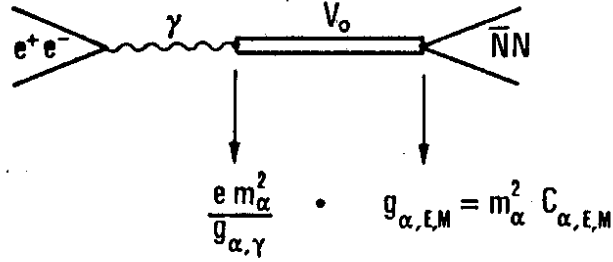
*fig.1*

letters S and V refer to the $V_0$ isospin; $g_{S,E}$, $g_{S,M}$ or $g_{V,E}$, $g_{V,M}$ are the coupling constants of $V_0$ to the nucleon, $em^2/g_{S,\gamma}$ or $em^2/g_{V,\gamma}$ are the coupling constants of the photon to the vector meson (of mass m). The Sachs form factors are related to the Dirac-Pauli form factors,

$$G_{E,i} = F_{1,i} - \frac{q^2}{4M^2} F_{2,i} \qquad\qquad G_{M,i} = F_{1,i} + F_{2,i}$$

with i=p (proton) or i=n (neutron), and these to the isoscalar and isovector form factors:

$$F_{1,i} = F_{1,S} \pm F_{1,V} \qquad\qquad F_{2,i} = F_{2,S} \pm F_{2,V}$$

the positive sign holding for the proton and the negative one for the neutron. Finally the four isospin form factors are expressed as sums over the known vector mesons:

$$F_{1,\alpha} = \sum_j \frac{m_j^2}{m_j^2+q^2} C_{j,E} \qquad\qquad F_{2,\alpha} = \sum_j \frac{m_j^2}{m_j^2+q^2} C_{j,M}$$

Here $\alpha$ stands for S or V; when $\alpha$=S the sum runs over the isoscalar mesons $\omega, \varphi, ...,$ when

$\alpha=V$ over the isovector mesons $\rho$,....; the constants $C_{\omega,E}$, $C_{\omega,M}$, $C_{\rho,E}$,.... are defined as shown in fig. 1. In the time-like region $m^2+q^2$ is changed into $m^2+q^2+im\Gamma$, taking into account the width of the vector mesons. For $n$ vector mesons there are $2n$ unknowns; the constraints are the four conditions about the form factors at $q^2=0$ and also the well established experimental result that $(dG_{E,n}/dq^2)_{q^2=0}=0.5$; we are then left with $2n-5$ unknowns.

This kind of fit is able to reproduce the space-like data, provided that besides $\rho,\omega,\varphi$ also $\rho'$ and $\omega'$ are included. In fig. 2 is shown the result of such a fit in the time-like region as well as the existing experimental points, represented as cross section values or form factors values, under the assumption $|G_E|=|G_M|$. In these calculation the neutron form factor comes out about one order of magnitude larger than the proton one; this appears as a general feature confirmed by many authors[1,3]. However such a measurement has never been attempted, as pointed out before.
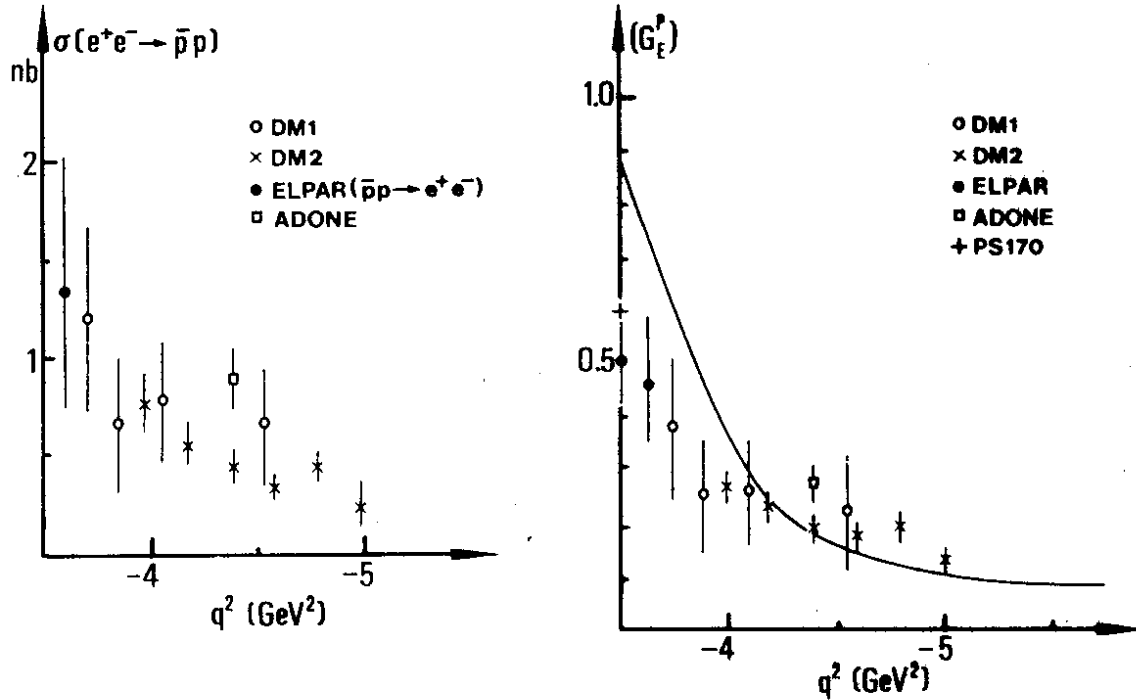


o    B.Delcourt et al., PL, 86B, 395 (1979)
x    D. Bisello et al., NP, B224, 379 (1983)
•    G. Bassompierre et al., PL, 68B, 477 (1977)
◻    M. Castellano et al., NC 14A, 1 (1973)

*fig.2*

It should be said that the VDM approach cannot be considered as satisfactory already at a computational level: since the number of poles is not fixed, and for some of them the experimental evidence is scarce, it is clear that with more free parameters a ficticious agreement with data can be found. On more general grounds it would be preferable a sounder approach: the electric and magnetic distributions of the nucleon, whose mathematical expressions are the form factors,

should be accounted for in terms of quark properties and probability density distributions.

In any case, while calling for a better theoretical frame, it appears mandatory to complete the precise measurements of such fundamental processes as the scattering of charged leptons off the nucleon and of the corresponding annihilation channels.

## 2. The choice between $e^+e^- \rightarrow \bar{n}n$ and $\bar{n}n \rightarrow e^+e^-$

The more conventional way to obtain the neutron e.m.f.f. in the time-like region is via the reaction $e^+e^- \rightarrow \bar{n}n$; another possibility is to use an antineutron beam on a deuterium target, i.e. $\bar{n}n \rightarrow e^+e^-$. We shall compare the event rates of these two channels.

Let us consider an electron-positron storage ring with a luminosity that is some factor times $10^{29}$, $L=F \cdot 10^{29} cm^{-2} s^{-1}$; the cross section for $e^+e^- \rightarrow \bar{n}n$ is not known and we assume that it is the same as for $e^+e^- \rightarrow \bar{p}p$. About 70 MeV above the threshold $\sqrt{s}=1.95$ GeV, $\sigma_1 \approx 1 nb$ and the number of events is $F \cdot 10^{-4} s^{-1}$. Since F should range from 3 to 10, $N_{ev}=(0.3 \div 1) \cdot 10^{-3} s^{-1}$ in the whole solid angle.

For the $\bar{n}n$ initial state the same value of $\sqrt{s}$ is reached at an incident momentum around 0.55 GeV/c and the corresponding cross section, according to (1.5), is $\sigma_2 \approx 14 nb$; the number of events with a liquid deuterium target 30 cm long is $n_{ev} \approx 10^{-8} N_0 s^{-1}$ in the whole solid angle; $N_0$ is the number of incident antineutrons per second. A clean way to produce antineutrons is from reaction $\bar{p}p \rightarrow \bar{n}n$; one can immagine a $\bar{p}$ beam impinging on a liquid hydrogen target, placed in a strong magnetic field; at $0°$ and at a given distance from this target there is the deuterium target. Charged particles are swept away by the magnetic field and good events originated by antineutrons in the second target are tagged by time-of-flight. We assume that the $\bar{n}$ production target is 30 cm long, that there are $10^6 \bar{p}/s$, that the solid angle subtended by the second target is $10^{-2}$ sterad and that $(d\sigma/d\Omega)_{LAB} \approx 10 mb/sterad$, according to published data: we obtain $N_0 \approx 130 s^{-1}$ and consequently $n_{ev} \approx 1.3 \cdot 10^{-6} s^{-1}$.

Even with major improvements in $\bar{p}$ intensity and in acceptance the $e^+e^-$ approach looks more realistic and certainly easier, avoiding the $D_2$ target complication.

## 3. Machine performances

A substantial improvement program is under way on both LNF accelerators, the 350 MeV injector Linac and the 1.5 GeV storage ring Adone, to upgrade their performances in view of resuming operation in the $e^+e^-$ collision mode.

On the Linac, the present gun providing 4 μs long 500mA pulses is being replaced by a

triode gun of the same type of that used for LEP, capable of delivering short and intense 10A, 10ns current pulses: this will increase the peak positron production and obtain positron injection in the range of 4mA per minute at 1.5 Hz. The gun and buncher system have a somewhat novel design since the four cavity buncher is less sensitive to space charge than conventional designs and has a very good capture efficiency. The emittance is also improved compared to the LEP Linac gun.

The Adone fifteen year old stainless steel vacuum chamber is being replaced by a new one with lower impedance and carrying a modern beam position monitoring system.

Finally, the ring 51.4 MHz RF system will be upgraded. Computer simulations of resonant discharges have shown how to eliminate high voltage multipactor thresholds in aluminum cavities by proper design and surface treatments.

## 3.1 Luminosity

The luminosity for head-on collisions in a storage ring with gaussian beams is given by the expression.

$$L = \frac{k i_b^2}{e^2 f_0 \, 4\pi \sigma_x \, \sigma_y} \tag{3.1}$$

where $k$ is the number of bunches per beam, $i_b$ is the bunch current, $f_0$ the revolution frequency, $\sigma_x$ and $\sigma_y$ the standard deviations of the transverse beam dimensions at the interaction point ($x$ is the radial coordinate and $y$ the vertical one).

During the interaction, due to the space charge forces, each beam is affected by the other and this leads to a storable current limitation for both beams. In the simplest beam-beam interaction model, the linear one, the effect of one beam on the other is simulated by a thin lens with an inverse focal length given by the interaction parameter $\xi$ that measures the interaction intensity[4]:

$$\xi_j = \frac{i_b r_e b_j}{2\pi e f_0 \, \gamma(\sigma_x + \sigma_y)\sigma_j} \tag{3.2}$$

where $j$ stands for $x$ or $y$ and $r_e$ is the classical electron radius, $\gamma$ the relativistic factor, $\beta_x$ and $\beta_y$ the betatron functions at the crossing point.

This lens gives a linear tune-shift $\Delta v$ with respect to the unperturbed tune of the machine that is related to the parameter $\xi$ by

$$\cos 2\pi(v_0 + \Delta v) = \cos 2\pi v_0 - 2\pi\xi\sin 2\pi v_0 \qquad (3.3)$$

$v_0$ being the betatron tune "per crossing". A related effect is the variation of the beta function $\beta_0$ at the interaction point:

$$\beta\sin 2\pi(v_0 + \Delta v) = \beta_0\sin 2\pi v_0$$

From measurements on Adone and other storage rings, a limit is found on the maximum $\Delta v$ value per crossing. When approaching the integer tune, because of relation (3.3) the limiting $\xi$ may increase for the same value of the limiting $\Delta v$. This effect increases the limit of the current per bunch so that it is possible to improve the luminosity. At Adone, to inject more current per bunch (see relation (3.2)), the full coupling ($v_x = v_y = 3.05$) working point was chosen.

Luminosity measurements have shown for an energy of 1 GeV/beam a peak luminosity of $L = 3 \cdot 10^{29} cm^{-2}s^{-1}$ with $i_b = 17mA$ and $k = 3$ [5]. Below 1GeV $L$ falls proportionally to $\gamma^7$, while above 1 GeV it levels off at the given value.

A possible way to improve the luminosity in Adone is to lower the $\beta_y$ value, that for the normal configuration is $\approx 3m$. A new machine optics has therefore been calculated[6] with four independent families of quadrupoles per cell, instead of two; this changes the machine periodicity from 12 to 6. With this solution the operating tune is still the standard one (ranging from 3.05 to 3.2): it will be possible to inject on the normal configuration and then to go to the low-$\beta$ one without problems. The betatron functions at the interaction point are

$$\beta_x = 4.5m \ , \ \beta_y = 1.0m$$

instead of the standard values $\beta_x = 9m$ and $\beta_y = 3m$.

For the colliding beam physics Adone was always operating with three bunches per beam, due to the presence of three experiments. With only one apparatus, now it will be possible to operate with one bunch ($k = 1$). This can reduce by a factor 3 the cosmic ray background. In

addition for the same value of $\xi$, more current can be stored in the single bunch mode, that is $i_b$ can increase, but the total current is reduced with a corresponding reduction of machine background and of those instabilities which have a threshold in total current. With one bunch there are no coupled - bunch instabilities, which were cured before with a special high frequency cavity.

As an estimate of the tune-shift $\Delta v_x$ and $\Delta v_y$ with one bunch it is possible to refer to some strong beam-weak beam measurements[7] that give an upper limit of $\Delta v$ about a factor 2 larger than the three bunches limit.

A very important parameter that affects the average luminosity is the accumulated beam lifetime. In Adone, during the last years, the lifetime has dropped from the 8-10 hours of the colliding beam operation to the 2-4 hours of the synchrotron light operation. Several factor have contributed to this worsening: the vacuum chamber is old (>15 years), there are losses due to the deterioration of its internal surface and it is possible to heat it only partially. The installation of a new pre-vacuum system and the installation of a new, smaller and almost completely bakable beam pipe, with especially treated internal surface, will rise again the beam lifetime to the old values.

As a conservative conclusion one can foresee, after the running in period, a peak luminosity at least at the level of $3 \cdot 10^{29} \mathrm{cm}^{-2}\mathrm{s}^{-1}$ eventually rising to $10^{30} \mathrm{cm}^{-2}\mathrm{s}^{-1}$.

## 3.2 Source length

In a colliding beam experiment the shorter is the interaction region of the beams the larger is the solid angle covered by the apparatus and the better the cosmic ray and machine background rejection. The effective source length for the apparatus is given by

$$\sigma_{eff} = \frac{\sigma_e}{\sqrt{2}}$$

and $\sigma_e$, the r.m.s. bunch length, has the espression

$$\sigma_e = 1.6 \cdot 10^3 \left( \frac{\alpha_c}{h V_{RF} \cos\phi_s} \right)^{1/2} E^{3/2} \, \mathrm{cm} \qquad (3.4)$$

where $\alpha_c = 0.064$ is the momentum compaction factor, $E$ the beam energy in GeV, $h$ the RF

harmonic number, $V_{RF}$ the RF peak voltage in KV, $\phi_s$ the synchrotrons phase. This bunch length is current independent up to the anomalous bunch lengthening threshold, given in terms of average current by

$$<I_{th}> \cong 1.75 \cdot 10^5 \left( \frac{\alpha^3_c E^9}{hV_{RF}\cos\phi_s} \right)^{1/2} \frac{1}{(Z/n)_c} \frac{<mA>}{bunch}$$

where $(Z/n)_c$ is the longitudinal coupling impedance.

The beam-vacuum chamber walls interactions, with all discontinuities, parasitic RF cavities, instrumentation, etc, can be described by a broad-band resonator with $Q \approx 1$ and resonant frequency almost equal to t he minimum cut-off frequency $f_c$ of the pipe for TEM (in Adone $f_c \approx 1$ GHz). The quantity $(Z/n)_c$ is the broad-band resonator impedance at $f_c$ divided by the mode number $n=f_c/f_0$ (in Adone $f_0=2.86$ MHz) and it is almost constant for $f<f_c$, that is the case of the bunch frequency spectrum of Adone.

$(Z/n)_c$ is a measurement of the discontinuity of the beam pipe: if it is small the beam sees a continuous pipe. Indirect measurements of $(Z/n)_c$ for Adone give a value $\approx 20\Omega$; after the beam pipe substitution a value $\approx 6 \div 10\Omega$ is foreseen. In this case $<I_{th}>$ will be rised and the head-tail instabilities should decrease too.

In the anomalous lengthening regime the r.m.s. bunch length is[8]:

$$\sigma_1 = 15.5 \left[ \left( \frac{Z}{n} \right)_c \xi \right]^{1/3} cm$$

where $\xi$ now is the Chao-Gareyte scaling parameter,

$$\xi = \frac{2\pi<i_b>}{h\,V_{RF}\cos\phi_s} \frac{<mA>}{KV}$$

and $<i_b>$ is the average current per bunch.

In fig. 3 the effective source length $\sigma_{eff}$ is plotted, for different energies and different RF systems, as a function of the bunch current. A practical figure of $\sigma_{eff}=8cm$ can be assumed, with $<i_b> \approx 50mA$.
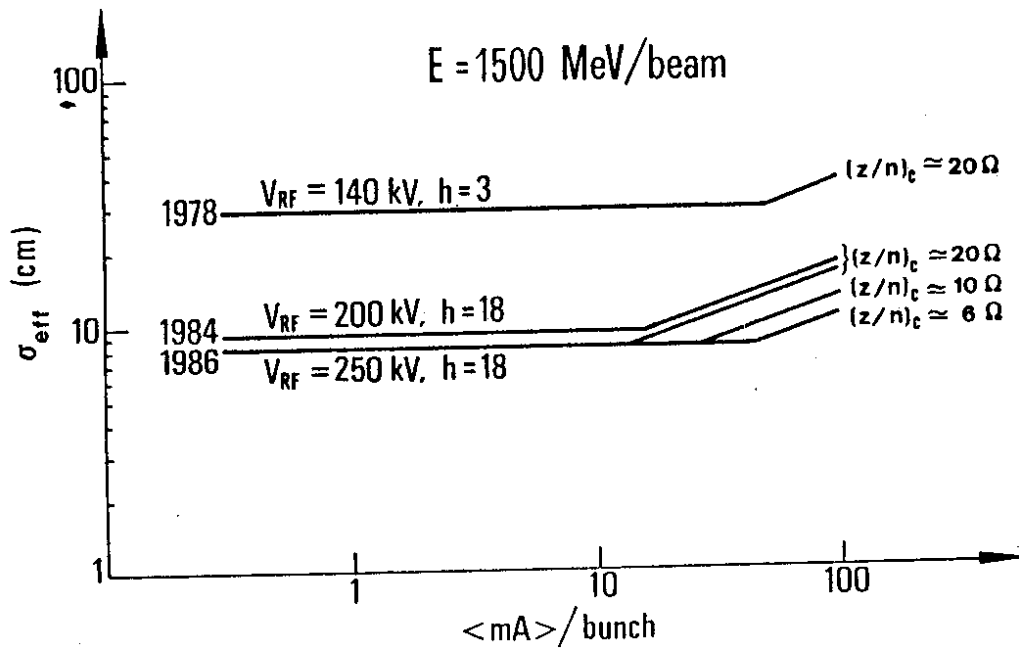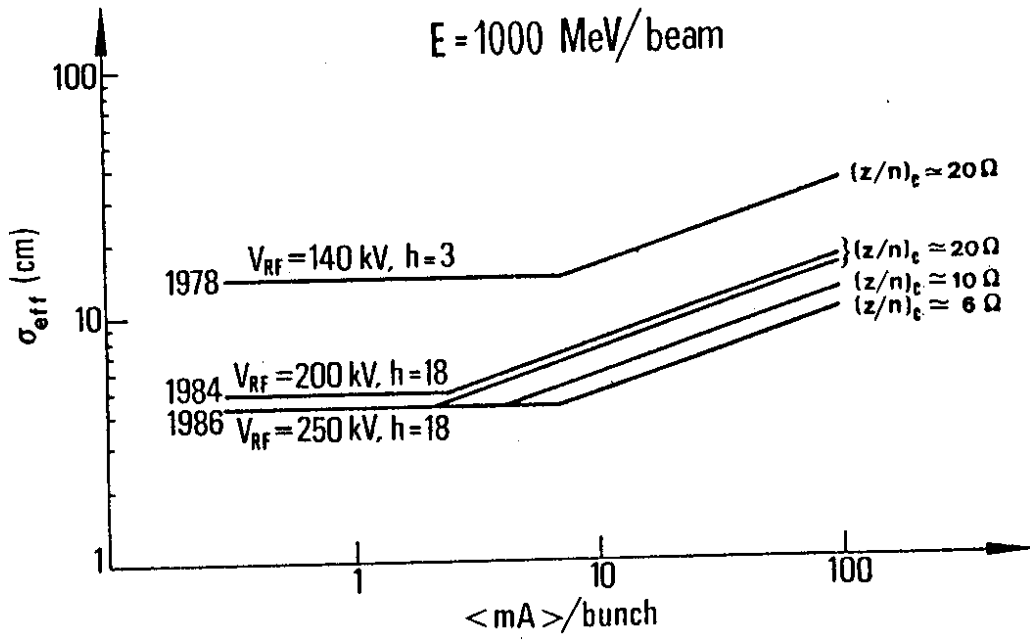
*fig.3*

## 3.3 Injection

When Adone was operating as a colliding beam facility the injection time was between 10 and 15 minutes. The new RF cavity, operating at a higher frequency (51.5MHz), has a large influence on the injection efficiency: since the harmonic number is changed from 3 to 18, with a Linac pulse longer than the revolution time ($4\mu s$ instead of 350ns ) the single bunch injection efficiency is reduced by approximately a factor 6. With the new Linac electron gun the pulse length (10ns) will be shorter than the RF bucket size (19.4ns) and the whole pulse will fall into the stable longitudinal phase space and single turn injection will ensure larger efficiency.

With the foreseen peak gun current the time needed to inject three positron bunches will not change with respect to the old RF configuration while single bunch injection time will be shorter by a factor 3.

## 3.4 Luminosity measurement

A measurement of the storage ring luminosity L is required for two main reasons:
   1) L relates the counting rate of $\bar{n}n$ or other reactions to their cross section;
   2) L must be continuously optimized during data collection.

In order to achieve the first goal it is necessary to measure the counting rate of a reaction with well known cross section, which must be much larger than the $\bar{n}n$ one, so that the statistical error on L can be neglected with respect to the $\bar{n}n$ counting rate uncertainty. It is convenient to perform the L measurement at the same time and with the same experimental set-up of the main reaction, collecting for instance wide angle $e^+e^-$ events; with this procedure one has the same dependence on the longitudinal and transverse size of the source and approximately the same detection efficiency.

The characteristics of an apparatus designed to fulfill the second requirement are completely different: the storage ring parameters must be continuously tuned to maintain the conditions of maximum L: a fast measurement is therefore needed, capable of observing L variations of less than 10% in a few seconds. To avoid systematic errors the experimental set-up should be insensitive to the position and length of the source.

Three processes can be considered: small angle $e^+e^-$ scattering, single bremsstrahlung (SB, $e^+e^- \rightarrow e^+e^-\gamma$) and double bremsstrahlung (DB, $e^+e^- \rightarrow e^+e^-\gamma\gamma$). The first and the third reaction suffer from low counting rate, typically 1Hz at Adone; in addition the $e^+e^-$ scattering is very

sensitive to the source size and the DB process has a strong background from accidental coincidences of SB events and bremsstrahlung events on the residual gas (GB).

The best reaction for a fast L measurement is indeed single beam-beam bremsstrahlung because of its large cross section and small angular aperture of the emitted photons (99% of these stay within ±5 mrad at 1GeV). The counting rate for a luminosity of $3 \cdot 10^{29} \mathrm{cm}^{-2} \mathrm{s}^{-1}$ is plotted in fig. 4 as a function of the threshold energy of the photon detector; also shown is the GB counting rate; if an increase of luminosity is achieved in the low-$\beta$ configuration, SB scales linearly with L while GB scales linearly with the stored current.
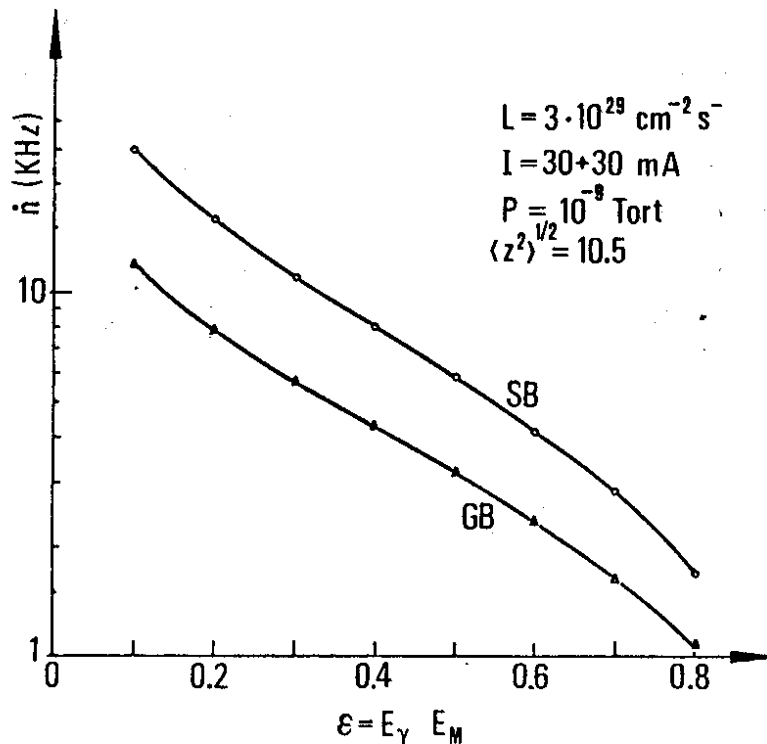


*fig. 4*

The GB events are a background that cannot be distinguished from SB events: they have the same energy spectrum and the same angular aperture and direction; a statistical subtraction is therefore needed. To this purpose an additional bunch, with much less current than the standard ones, is injected; the counting rate measured in coincidence with its passage through a straight section is due only to GB events and can be subtracted under the assumption that the GB rate from a given straight section is proportional only to the current in a given bunch.

This procedure was troublesome during the first generation experiments at Adone, because the RF system of the ring was operating at the third harmonic of the revolution frequency and the presence of four experiments on the ring at the same time required the injection of three e- and three e+ bunches, so that all the stable phases in the longitudinal phase space of the ring were filled. It was then compulsory to measure SB with three bunches of e- and two of e+,

reducing the total luminosity. With the present RF cavity, operating at 51.4MHz at the 18th harmonic, this problem does not exist.

The experimental set-up consists of two shower counters with a veto scintillator in front for the rejection of the electron background. In the system operating during the first generation experiments[9] the counters were sandwiches of forty 3mm thick scintillators separated by 3mm thick lead plates; the transverse size was 160x160mm$^2$, dictated by the DB measurement that was performed at the same time. A possible alternative to the sandwich is a cristal counter (NaI or BaF$_2$) whose energy resolution is much better. The energy threshold, determined by discrimination of the pulse heigth of the shower counter, is measured by a comparison of the experimental spectrum with the theoretical one[9].

The schematic layout of the set-up is shown in fig. 5; counter SW1 is placed on the prolongation of the $\overline{n}n$ straight section at $\approx$6m distance from the interaction point on the opposite side of the PULS synchrotron radiation beam line. The bremsstrahlung photons pass through a special vacuum chamber in the magnet, which has a thin stainless steel window, $\approx$1mm thick, perpendicular to the direction of the photons. Counter SW2 can be installed on the prolongation of any straight section of Adone; in fig. 5 for instance it looks at the wiggler straight section, in the opposite direction of the synchrotron radiation beam line.



*fig.5*

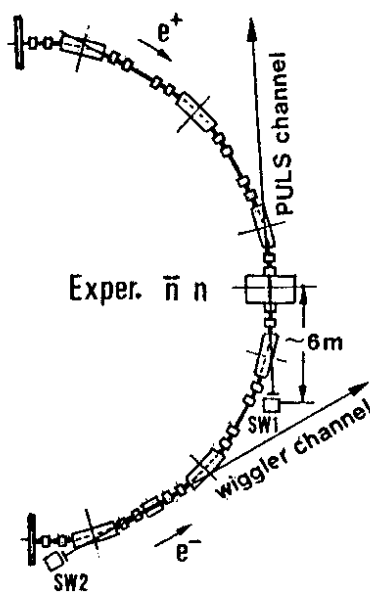In order to describe how the statistical background subtraction is performed and to estimate its random error, let us assume to have one bunch of e$^+$ and one of e$^-$, both with 30mA current, crossing with a luminosity L=3·10$^{29}$cm$^{-2}$s$^{-1}$ in the center of the $\overline{n}n$ straight section. As we have already said, in addition to the e$^+$ bunch travelling in the direction of SW1 and SW2

(fig.5), which we call bunch A, a second bunch B is injected with a smaller current $i_B = i_A/f$. It is assumed that bunch B does not cross the $e^-$ bunch, as bunch A does, in the low-$\beta$ section of the high luminosity configuration. The SW1 counting rate is

$$n_{1A} = n_{SB1A} + n_{GB1A}, \qquad n_{1B} = n_{GB1B}.$$

In the second straight section bunches A and B do not cross the $e^-$ bunch and the SW2 counting rate is

$$n_{2A} = n_{GB2A}, \qquad n_{2B} = n_{GB2B}.$$

The luminosity is proportional to $n_{SB1A}$ through a function $K(e)$ of the relative threshold energy $\varepsilon = E/E_{beam}$:

$$L = K(\varepsilon) n_{SB1A} = K(\varepsilon)(n_{1A} - n_{GB1A}).$$

Assuming that

$$\frac{n_{GB1A}}{n_{GB1B}} = \frac{n_{GB2A}}{n_{GB2B}} = \frac{i_A}{i_B} = f,$$

$$L = K(\varepsilon)(n_{1A} - n_{GB1B} \frac{n_{GB2A}}{n_{GB2B}}) = K(\varepsilon)(n_{1A} - n_{1B} \frac{n_{2A}}{n_{2B}}).$$

With the assumption that $n_{2B} = n_{1B}$, and $n_{2A} = f n_{2B} = f n_{1B}$, the statistical error on L comes out to be

$$\Delta L = K(\varepsilon) [n_{1A} + (2f^2 + f) n_{1B}]^{1/2}$$

and the relative error on the luminosity is

$$\frac{\Delta L}{L} = \frac{[n_{1A} + (2f^2 + f)n_{1B}]^{1/2}}{[n_{1A} - fn_{1B}]}$$

The counts per second can be read from fig. 4 (the GB rate from the "small" bunch has to be scaled by a factor f). Taking $\varepsilon=0.2$ and a measuring time of 10s, the relative error is $0.9 \cdot 10^{-2}$, for $f=10$.

We have assumed SW1 and SW2 of the same kind. However it is not necessary to have for SW2 the same linearity and resolution as SW1, since the only requirement for SW2 is the measurement of the ratio between the GB rates of the two bunches A and B, i.e. of the f ratio. Linearity and energy resolution must be good for SW1 to ensure a good fit of the photon spectrum for the determination of the threshold energy of the collected photons and consequently of the function $K(\varepsilon)$.

## 4. The detector

The proposed apparatus consists in principle of dedicated parts with separate functions, i.e. the $\bar{n}$ detector, the n detector, the central tracking detector and the cosmic ray shield. In practice some of these functions overlap, but in the following description we keep the distinction; the cosmic ray shield is discussed in section 5.

## 4.1 The $\bar{n}$ detector

An efficient $\bar{n}$ detection can be accomplished by means of annihilation in matter, exploiting the many prongs topology of the event. In a suitable detector the annihilation vertex is reconstructed and the time-of-flight (TOF) measured, thus yielding a complete kinematical identification of the $\bar{n}$. This concept has been valuably applied by the PS178 experiment at LEAR that measures the forward cross section of $\bar{p}p \rightarrow \bar{n}n$ and some subsequent reactions initiated by $\bar{n}$'s[10]. A similar structure has been chosen for the Adone experiment.

The main element is the following submodule:

- iron plate (5mm thick) as main converter
- limited streamer tube chamber (1cm$^2$ cell) as track detector [11].

This is repeated four times and then there is a

        - scintillation counter hodoscope (20mm thick) for trigger and TOF measurement.

The full module is again repeated four times; after the last hodoscope two more LST planes are added. Geometrically the detector has a octagonal shape (see fig. 6); mechanically the octants are not independent, but arranged in four supermodules that have individual support frames and can be moved on rails in order to open the apparatus (see fig. 7)



*fig. 6*



*fig. 7*

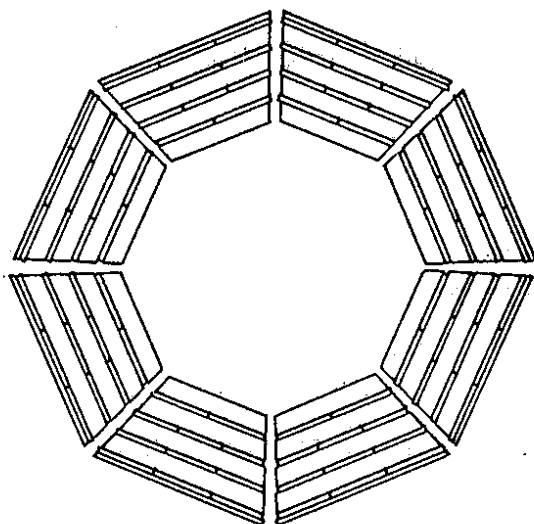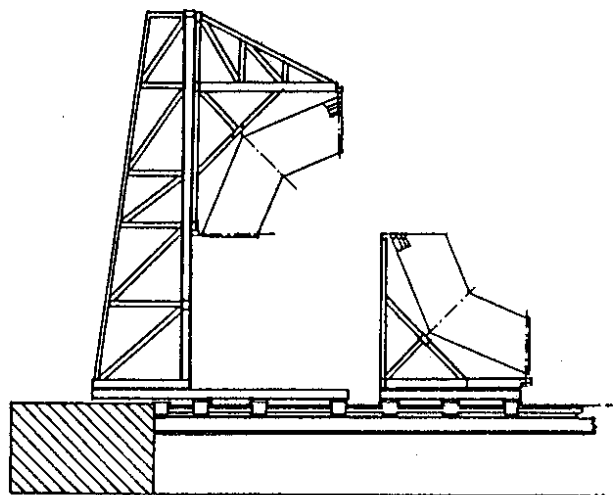Coming to a more detailed description of the active components, the LST chambers have basic modules with 8 or 7 cells suitably arranged as to leave as little dead space as possible. They are read out digitally with strips along the wires (1cm pitch) and across the wires at 90° (1.2cm pitch); we intend to use the new SGS integrated electronics . All relevant figures for the LST chambers are given in Table 1.

# TABLE 1

## antineutron detector

one sector = two octants
18 planes of LST, useful wire length 2.4 m or 1.9 m
longitudinal channels = wires 2752
tranverse channels 3600
total number of channels long. 11008, trans. 14400

## neutron detector

one sector = two octants
9 planes of LST, useful wire length 1.9 m
longitudinal channels = wires 832
tranverse channels 1440
total number of channels long. 3328, trans. 5760


In one octant there are 11 counters of slightly different sizes, always for dead space reasons; the scintillating material is NE110; all counters are viewed on both ends by THORN-EMI 9813KB photomultipliers. In Table 2 we list the relevant numbers.


# TABLE 2

## antineutron counters

one octant       11 counters
         5 counters    $2400 \times 330 \times 20$ mm$^3$
         3 counters    $2400 \times 293 \times 20$ mm$^3$
         3 counters    $2400 \times 258 \times 20$ mm$^3$
(in two octants out of eight the length is 1900 mm)
total 88 counters, 176 light guides and photomultipliers

The sensitive length along the straight section is approximately 2.4m; however the two lower octants have shorter tubes and scintillators ($\approx 1.9$m) because of interference with the quadrupole supports.

We expect to achieve a spatial resolution better than 5mm for the annihilation vertex coordinates and a TOF resolution around 0.8 - 0.9ns.

## 4.2 The n detector

Neutron detection is a more difficult task if one wants to preserve timing and position requirements at about the same level as for antineutrons. We have adopted the scintillation counter hodoscope solution, where the scintillator acts as converter as well as active material: neutrons are detected when they scatter off the quasi-free protons in the scintillator giving to the recoil protons enough energy to produce a detectable light pulse. In our energy range the detection efficiency is $\approx 1\%$ per cm of scintillator[12]; we plan to place three layers of counter hodoscopes with a total thickness of 15cm (see fig. 8), following the octagonal structure of the $\overline{n}$ detector. Scintillators and photomultipliers are the same as before; all relevant dimensions are given in Table 3.

The neutron interaction position is computed through the time and amplitude analysis of the pulse coming from the two photomultipliers viewing the same hodoscope element and this measurement has a typical resolution of few cm; the TOF resolution has approximately the same value as for the $\overline{n}$ detector.
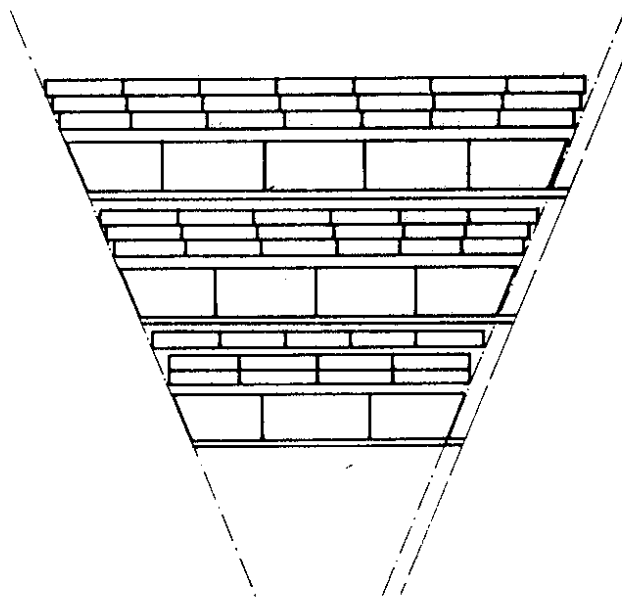


*fig. 8*

## TABLE 3

### neutron counters

one octant   12 counters,  each  1700 x 107 x 50 mm$^3$
total  96 counters,  192 light guides and photomultipliers

One notices in fig. 8 more layers of LST and at least one  iron absorber. Indeed  antineutrons annihilate also in the  n detector giving rise to many  prongs events that will give trigger, as explained in section 4.5; the LST chambers in the neutron detector are intended to recognize this kind of events. The iron absorber  has the main  task to shield the  neutron counter  from low energy photons (see section 4.6).

### 4.3 The central tracking detector.

Besides $e^+e^- \to \bar{n}n$ there are other processes that we are going  to  detect  for  their  physical interest  or for monitoring reasons  (see section  6); all  of these exibit charged  particles in  the final  state, originated  at the interaction  point or very  near to it  $(K_s^\circ, \Lambda^\circ, \Sigma)$. The aim of the central tracking detector  is  to measure with good accuracy the  charged particle tracks and  their vertices.  Moreover it will help in rejecting cosmic rays in collinear events, such  as $e^+e^-$ or $\mu^+\mu^-$, and to  better recognize $\bar{n}$  annihilations that send tracks back to  the central part of the apparatus.

As usual  in  the $e^+e^-$ colliding machines the best spatial resolution  is needed in the plane perpendicular to the  beam ($\phi$ view). In  this plane  in fact the beam cross section  is  $\approx 1 \cdot 0.1\,mm^2$ while  along  the beam ($\theta$ view) the interaction region has $\sigma \approx 10$ cm.  Another important point is to reduce  the  total  thickness  of  the detector and the thickness  and  the  diameter  of  the Adone vacuum pipe in order not to spoil the vertex reconstruction.

The new inox pipe has corrugated walls; the thickness is 0.3mm, the diametre 21cm and the length 1.2m; it leaves an  angle  $20° \geq \theta \geq 160°$ with  the  minimum  thickness. The stability under  vacuum  is  given  by  four tubes, 3cm in diametre, of carbon fibers, 1mm thick (see fig. 9).
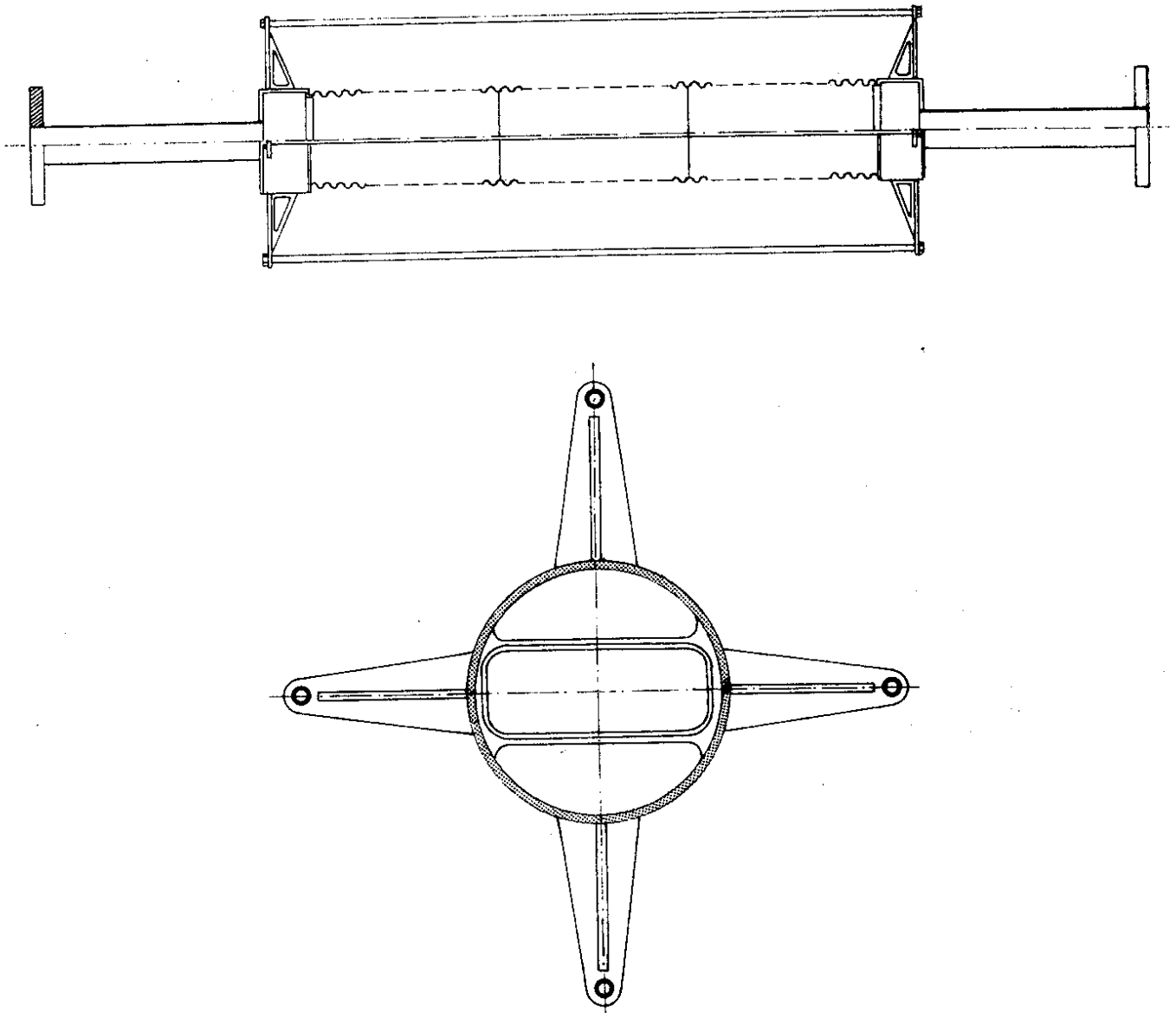
*fig. 9*

The tracking elements are the same LST as in the $\overline{n}$ detector; they are mounted parallel to the beam and their standard resolution, $\sigma \approx 2.3$mm, is not sufficient to reconstruct a vertex with an accuracy comparable to the beam dimensions. A simple technique to improve the resolution, while keeping the semplicity and reliability of the LST, is to read the drift time across the cell; preliminary results show that a resolution better than 0.5mm is achievable (private communication from the Padova group in the ZEUS collaboration at HERA).

The CTD is divided in two substructures, the first close to the pipe and the second just before the neutron counters; each substructure has four LST layers in order to record at least two points per track and to partially solve ambiguities when two tracks cross the same chamber in a layer.

The inner substructure has chambers with 7 cells that best fit the pipe diametre. The basic structure of cells and containers is still in PVC while the read-out strips and ground planes are made out of alluminized mylar (instead of alluminium) and are glued on 2mm rohacell strips. The cross section is shown in fig. 10.
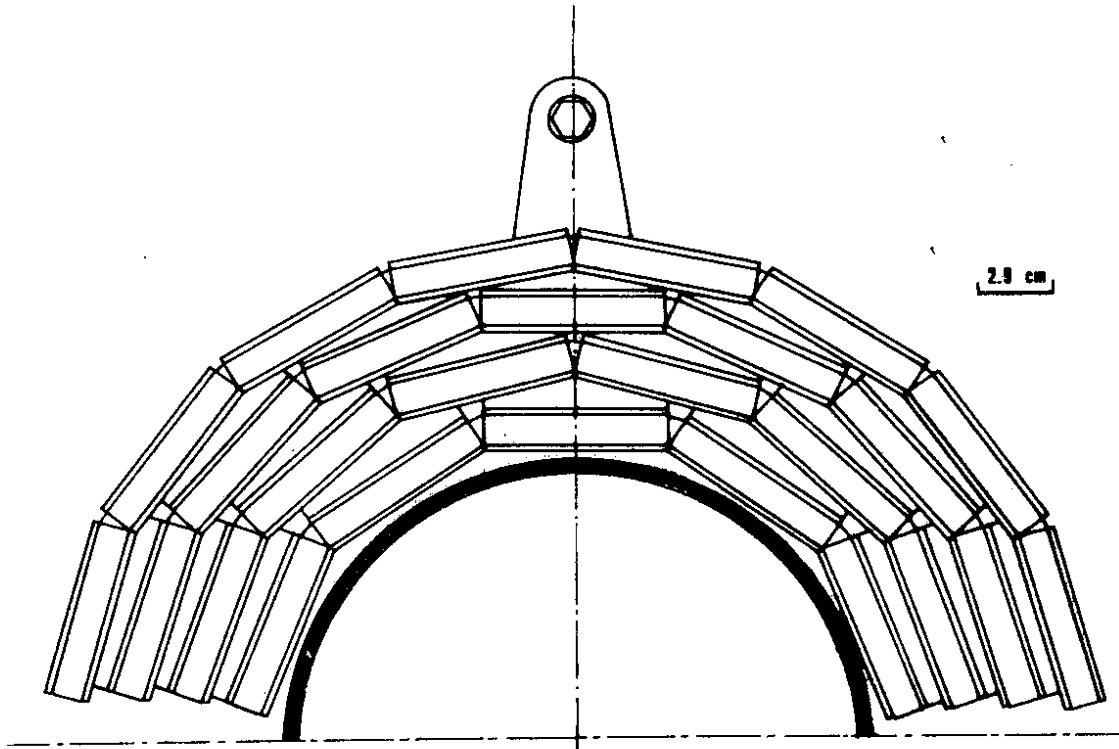


*fig.10*

The outer substructure has the same properties as the n detector chambers. In Table 4 are summarized all relevant figures of the central tracking detector; the number of TDC channels is low since we plan to read the time of the OR of 7 or 8 wires.

Between the pipe and the first tracking substructure there is a thin (5mm) scintillation counter hodoscope that is going to be used in anticoincidence for the $e^+e^- \rightarrow \bar{n}n$ triggers and in coincidence for the other triggers.

# TABLE 4

## central detector

| | | | |
|---|---|---|---|
| outer section | longitudinal channels = wires | | 720 |
| | transverse channels | | 2560 |
| inner section | longitudinal channels = wires | | 364 |
| | transverse channels | | 640 |

TDC channels  148

## 4.2  Acceptance, efficiency and event rate

The geometrical acceptance of the apparatus for a single particle originated in the interaction zone is $\approx 76\%$ of the total solid angle. For two collinear particles this figure becomes $\approx 74\%$ since there is an asymmetry in acceptance due to interference with the ring structure, as mentioned in section 4.1. The $\phi$ acceptance is $\approx 1.8\pi$ because of cracks, i.e. $\approx 90\%$ of the total. In the standard octant (2.4m long) $\theta$ spans the interval $32°\div 148°$, while in the shorter octants (1.9m long) the covered interval is $36°\div 144°$.

We plan to trigger on $\bar{n}$ annihilation, as explained in section 4.5, and for this trigger we take the one particle acceptance; the subset of events with $n$ identification has the two particle acceptance.

The calculation of the apparatus efficiency is more complicated. First of all one has to calculate the annihilation probabilities in the various materials and then set a criterium for the visibility of an event, i.e. a definition of what is the aspect of a $\bar{n}$ annihilation in the apparatus. Indeed, in our kinetic energy range that has a lower limit at $\approx 35$ MeV per $\bar{n}$ or $n$, the pions that come out as annihilation products are not very energetic; in the average the energy of $\approx 2$GeV released in the annihilation is divided amongst four or five pions, some of which are neutral; the charged ones, that must be at least two in order to define a vertex, do not give rise to long tracks, visible in many LST layers; moreover one has to take into account nuclear reabsorption effect. A conclusion, a fair amount of annihilation events do not give rise to spectacular and unmistakable topologies and a lot of care is needed to recognize them. These semiqualitative conclusions are confirmed by PS178 experience and by the first results of a Montecarlo calculations; at the present stage of simulation we can assume a detection efficiency for antineutron equal to $0.45\pm 0.10$. The distribution of $\bar{n}$ annihilation vertices in a plane perpendicular to the beam is shown in fig. 11, at two different energies.
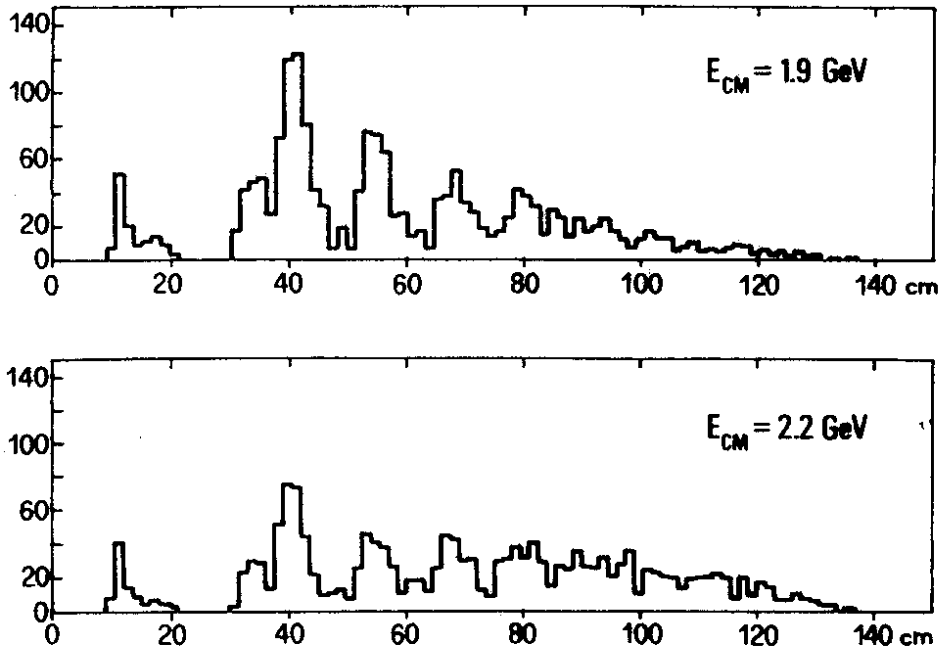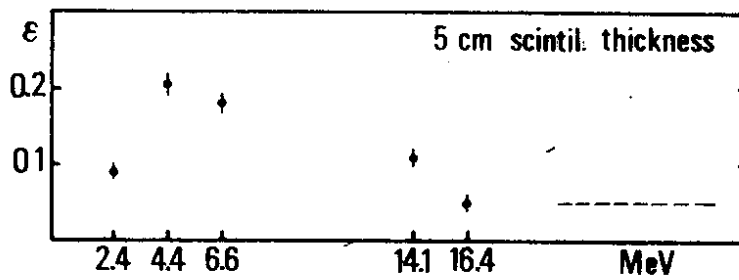
fig. 11



fig. 12

The neutron detection efficiency in NE110 scintillator has been measured by experiment PS178 and the result is shown in fig. 12. We assume a similar efficiency which flattens out to 0.01 per cm at higher neutron energies. The calculated percentage of $\bar{n}n$ events that, besides a $\bar{n}$ annihilation, have the neutron detected in the apparatus is P=0.17.

Summarizing the acceptance A and efficiency $\varepsilon$ figures and recalling the figure

$N_{ev}=(0.3\div1)\cdot10^{-3}s^{-1}$ given in section 2, we arrive at the following results:

number of events with a $\bar{n}$ annihilation=
$$A_1\varepsilon N_{ev} = (1.0\div3.4)\cdot10^{-4}s^{-1}$$
number of events with complete $\bar{n}n$ detection=
$$A_2\varepsilon N_{ev} = (1.7\div5.7)\cdot10^{-5}s^{-1}$$

## 4.5 Trigger

A good antineutron event at the trigger level is defined by the following requirements:

1) in coincidence with the RF signal there is a given number of $\bar{n}$ counter hits in one octant; a "counter signal" is given by the coincidence of the two photomultipliers viewing the scintillator;

2) there must be no signal in the veto counters surrounding the interaction region. Since $\bar{n}$ annihilations can occur also in the neutron counters, we ask similar requirements for such events.

This simple trigger can work if the noise of whatever origin does not exceed our readout capabilities. Indeed we have made machine background measurements at Adone, that are described in section 4.6. It is however possible to tighten the trigger rising the majority level from two to three hits in one octant and, if necessary, asking for a minimum numbers of hits in the LST.

When a trigger occurs we read out for all counters the hit pattern and the signal amplitudes and times. From the pattern we can see on line whether there has been a signal from a neutron counter opposite in the $\phi$ view to the octant that has triggered. It is left to the off line programs the TOF analysis that is the main tool to single out the $\bar{n}n$ events: indeed, when a $\bar{n}$ event occurs in the $\bar{n}$ counters, there is a time difference larger than 6ns between a relativistic particle and an antineutron; this figure is reduced to 3ns for events in the neutron counter. Also the correct association neutron-antineutron will be done off line, on the basis of TOF and collinearity.

Most of the modules employed in the trigger are commercially available CAMAC modules (Lecroy ECL-line), although some functions are performed in NIM standards. We are developping a special ECL module that makes the majority operation within a preselected window, i.e. there is an output signal only if the input hits i satisfy the condition $i_{MIN}\leq i\leq i_{MAX}$; all inputs are strobed and the module memorizes also the pattern of the hits.

Some details of the $\bar{n}$ trigger scheme are given in fig. 13; other possible triggers are discussed in section 6.
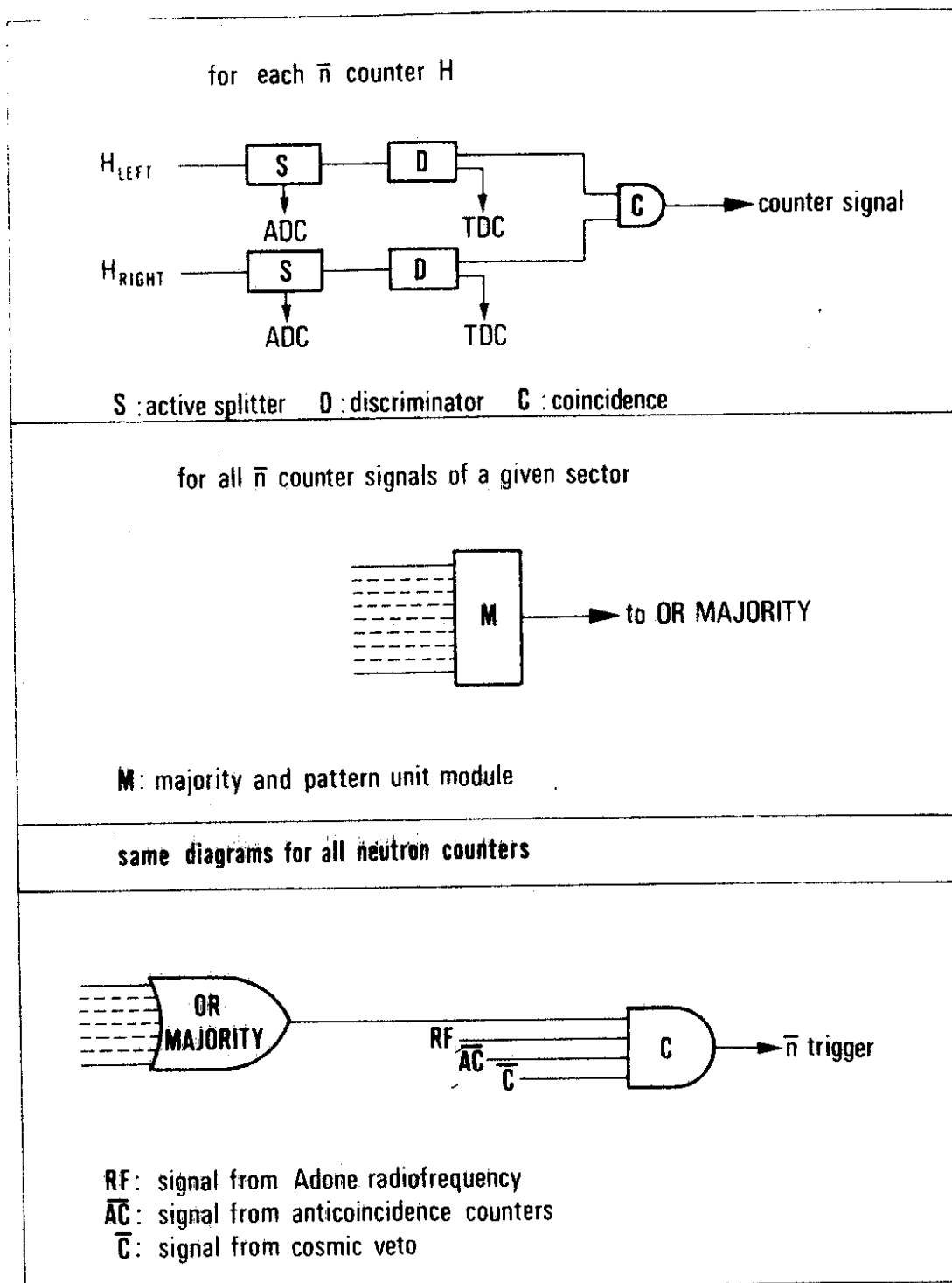
for each $\bar{n}$ counter H



$H_{LEFT}$ ─── S ─── D ─── C ──► counter signal
ADC      TDC

$H_{RIGHT}$ ─── S ─── D
ADC      TDC

S : active splitter     D : discriminator     C : coincidence

---

for all $\bar{n}$ counter signals of a given sector



M ──► to OR MAJORITY

M : majority and pattern unit module

---

same diagrams for all neutron counters



OR MAJORITY ──── C ──► $\bar{n}$ trigger
RF
$\overline{AC}$
$\overline{C}$

RF : signal from Adone radiofrequency
$\overline{AC}$ : signal from anticoincidence counters
$\overline{C}$ : signal from cosmic veto

fig. 13

## 4.6 Machine background tests.

In order to estimate the counting rate that is induced on the various counters by the machine radiation we have performed a test in a straight section of Adone with a circulating beam of 50mA at 1GeV. A 15cm thick lead shield was positioned at the beginning of the straight section, i.e. after the last quadrupole.

We have first simulated the veto hodoscope just putting on the pipe a 60x16 cm$^2$ scintillation counter, 2cm thick; the rate was 23 KHz that becomes 110 KHz for the whole hodoscope scaling with the are and the beam intensity (but not with the thickness).

The same counter has been used to simulate a neutron counter: we put it at 50cm from the beam axis, parallel to it and in three positions, outside and inside with respect to the beam in the orbit plane and below the orbit plane; the counting rate was respectively 5 KHz, 25 KHz, 2KHz. A real $n$ counter without any shielding should count about three times more.

A three counter coincidence telescope has then been used to further investigate the machine noise; the counter area was 15x15cm$^2$, the thickness 2cm. In the orbit plane at 30cm from the beam we tested the following positions:

    1) telescope axis parallel to the beam:

        500Hz on the inside, 200Hz on the outside;

    2) telescope axis orthogonal to the beam:

        250Hz on the inside, 4Hz on the outside.

Below the orbit plane, at 50cm from the beam and with the telescope axis orthogonal to the beam, we counted 14Hz.

Inserting 1.5 radiation length of lead between the counters the coincidence rate falls by at least two orders of magnitude. A veto counter around the pipe would have suppressed the rate by other two orders of magnitude.

We conclude that in any case these rates do not constitute a real problem for the apparatus, considering in addition that the vacuum will be better. The mechanical design of the neutron detector is such that it is possible to insert absorbers before the first layer of counters and also between the layers. We are presently calculating the effect of these absorbers on neutron and antineutron detection.

## 4.7 Data acquisition

At each trigger the data acquisition system has to read out the content of the following modules:

1) 400 ADC channels;

2) 400 TDC channels;

3) 200 Pattern units channels in the majority modules (see section 4.5);

4) Scalers;

5) LST controllers: we foresee five controllers, each with 8 parallel 1024 bit read out lines;

6) LST TDC from the central detector.

The total readout time is ≈5ms per event.

These data are transferred to a DEC Micro Vax II computer with 3 Mbyte memory and two 70 Mbyte disks, connected via ETHERNET to the DEC VAX 8600 computer of the LNF computing center. The events are recorded on the Micro Vax disk and periodically written on magnetip tape at the central computer. All groups in the collaboration have access to the information via INFNET.
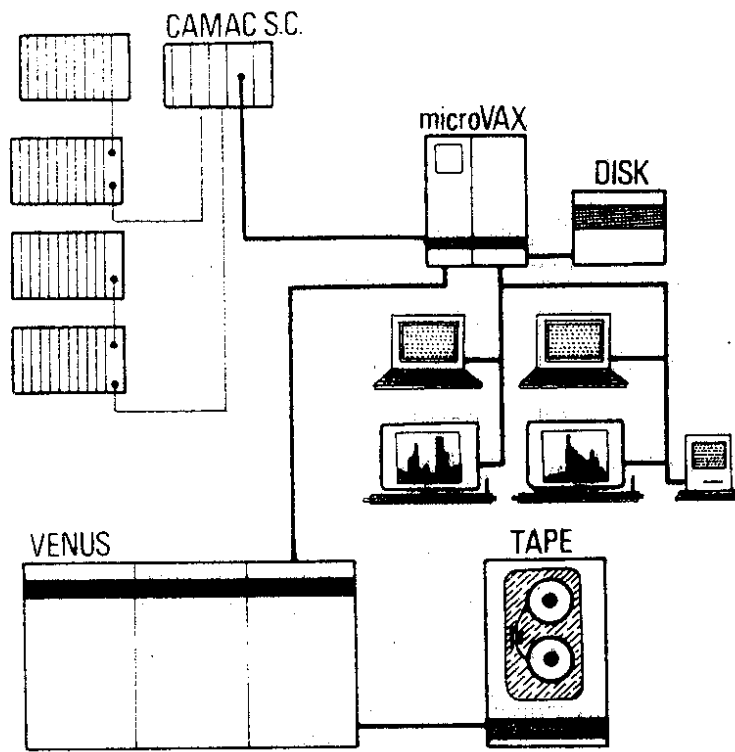
Two other tasks are independently performed: the luminosity and the apparatus monitoring. The scheme is essentially the same: a CAMAC crate hosts the control modules under the supervision of a MACINTOSH personal computer; a link to the Micro Vax is provided via an auxiliary crate controller.

For the luminosity monitor the SW1 and SW2 counting rates are read out by scalers whose content is also displayed in the Adone control room for continuous adjustment. From time to time an absolute measurement of pulse heigth is performed in order to compare it with the theoretical spectrum (we recall section 3.4).

The apparatus monitor drives and controls all high voltage power supplies, checks the low voltages, drives the light diode system for counter and trigger calibration, performs the gas flow control.

The schemes concerning the various tasks of the data acquisition system are shown in fig. 14.

# FENICE DATA ACQUISITION

CAMAC S.C.

microVAX

DISK

VENUS

TAPE

# LUMINOSITY MONITOR ACQUISITION

ADC  SCALER  COINC  DISCRI  AUX CC  MAC CC
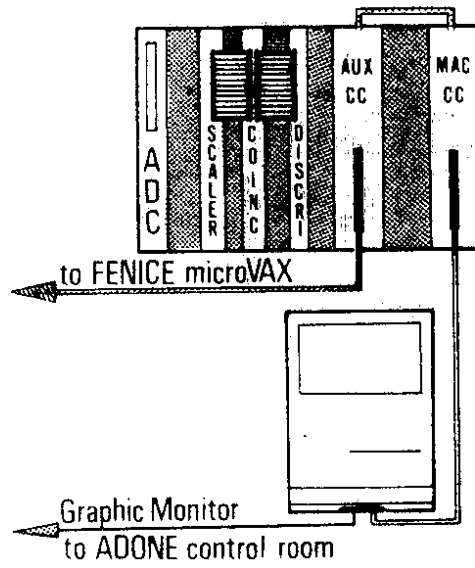
to FENICE microVAX

Graphic Monitor
to ADONE control room

*fig.14*

## 5. The cosmic veto

The process $e^+e^-\to\bar{n}n$ can be simulated by interactions of muons and neutrons coming from cosmic rays; although their rate is not high, still they can constitute a relevant background to $\bar{n}n$ events, whose rate is $\approx 10^{-4}s^{-1}$. To reduce this source of background a concrete hut will be built around the detector, covered by an active veto system. The latter detects with high efficiency in a large solid angle the charged cosmic particles and acts as anticoincidence in the trigger; it could also detect charged secondaries produced with a neutron in a primary cosmic radiation interaction. The concrete shield attenuates the neutron flux and helps in containing all particles from $e^+e^-$ interactions (with the exception of $e^+e^-\to\mu^+\mu^-$ events) that otherwise would lead to a self-veto; its thickness is 100 cm. The overall dimensions are shown in fig. 15.
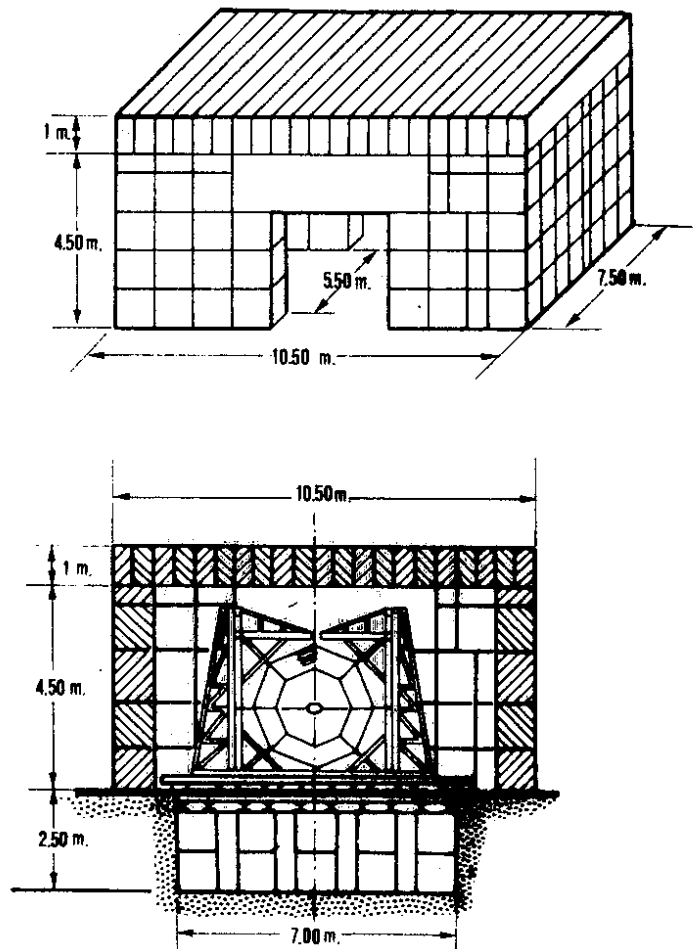


*fig.15*

## 5.1 Evaluation of rates and of rejection power.

The muon flux integrated over the apparatus gives a rate of $1500s^{-1}$ that is reduced to $150\ s^{-1}$ by the requirement of coincidence with the RF signal. The active veto cuts this rate: the rejection power depends on the inefficiency, that is of the order of 1% (see section 5.2) and on the area that cannot be covered, notably on both sides of the straight section along the beam direction, where the ring elements are situated. These windows correspond to a 3% inefficiency and the total inefficiency is 4%; the cosmic muon trigger has then a rate of $6s^{-1}$.

The off line analysis adds strong constraints: a many prong event originated by a muon in iron has a probability[13] as low as $0.7 \cdot 10^{-4}$; the off-line TOF analysis brings in another $2.8 \cdot 10^{-2}$ factor. The final rejection power is $2 \cdot 10^{-6}$, giving a rate of $1.2 \cdot 10^{-5}s^{-1}$ for muon events that mimic $\overline{n}n$ events.

The neutron flux integrated over the apparatus is estimated at $5s^{-1}$. In order to give triggers these neutrons must produce many prong events: according to their inelastic cross section in iron[14] and to the reduction factor due to the RF timing, the effective trigger rate is $2 \cdot 10^{-2}s^{-1}$. After the off line analysis the events that survive to the TOF cut have a rate $5.6 \cdot 10^{-4}s^{-1}$, too large with respect to the good event rate $(10^{-4}s^{-1})$. Due to the $\cos^8\theta$ dependence of the neutron flux[15], this can be considerably reduced just adding more shielding at small values; for instance a suitable loading of the concrete for $\theta \leq 25°$ attenuates the flux by a factor $\approx 70$ and the final rate of cosmic neutron events that mimic $\overline{n}n$ events is $0.8 \cdot 10^{-5}s^{-1}$.

Summarizing the results, the cosmic ray events give a trigger rate of $\approx 6s^{-1}$; after the analysis their contribution amounts to 20% of the signal $(2 \cdot 10^{-5}$ against $10^{-4}s^{-1})$.

This estimate has many uncertainty factors; for instance we have not applied efficiency cuts to the many prong events originated by cosmic rays, assuming that they are all detectable; in addition we have not considered the possibility that such events might present particular topologies, being originated by high energy particles. These aspects will be investigated experimentally running the apparatus without beam, that is in any case necessary in order to establish a statistical subtraction of the cosmic ray background.

## 5.2 The veto counters

The active detectors are resistive plane counters (RPC)[16] that we briefly describe. A strong electric field, $4 \div 5$ KV/mm, generated by two plane and parallel electrodes of high resistivity $(10^{11}\Omega cm)$, is applied to a 2mm gap filled with the gas mixture 69% Argon, 30% Butane, 1% Freon. The primary ionization electrons give rise to the process free

electron-avalanche-streamer in a time that is shorter than in any other gas detector and with very small fluctuations. The high resistivity of the electrodes and the UV photon absorption in the gas quenche the electrical discharge. The typical pulse height is 1V over 50Ω, the duration is 10ns and the time spread 1ns. These pulses are capacitively read out on aluminium strips 3cm wide that behave as transmission lines with 50Ω impedence.

The basic RPC module has dimensions $2 \times 1 m^2$; over this area the gap uniformity is kept by PVC cylindrical spacers.Two such modules are superimposed to form a double gap rigid structure; the details are shown in fig. 16.
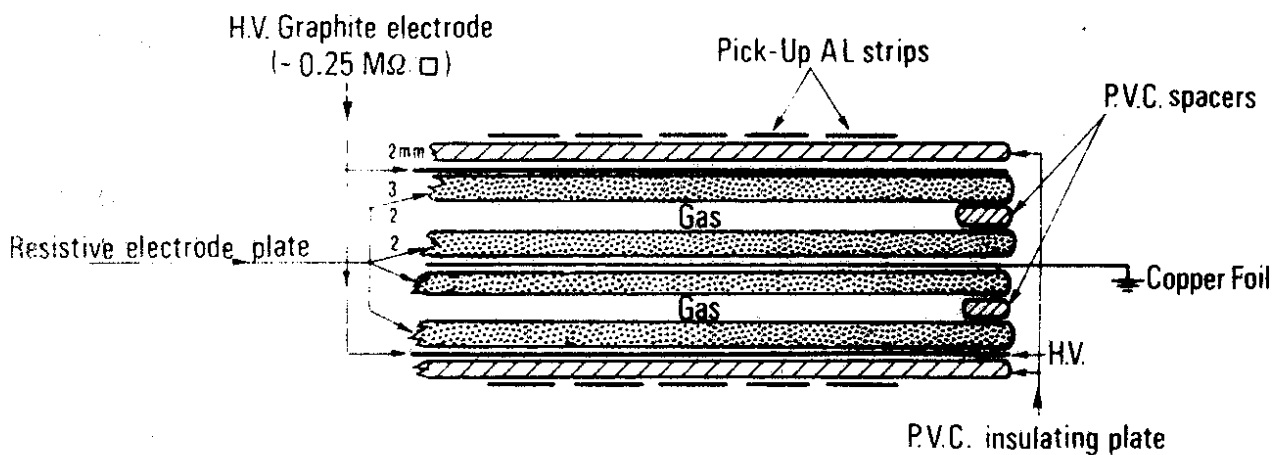


*fig. 16*

A veto counter is made with three of the above described double modules and has an area $6 \times 1 m^2$. It is read by 64 strips (32 per each sensitive plane) 6m long.

The intrinsic efficiency per plane is 97%; using the OR of the two superimposed planes the real efficiency is determined only by dead zones, i.e. the spacers and a 7mm wide region all along the sides of the counter. By suitable superposition of adjacent modules the inefficiency is essentially due to the spacers and amounts to ≈1%.

The natural frequency of RPC is ≈1KHz/$m^2$, the total surface is $2 \times 250 m^2$; the probability that a $e^+e^-$ event coincides within 30ns with a veto signal is 1.5%; this is the dead time effect due to the veto (with zero machine background).

The readout electronics is based on a 16 channel discriminator card (one channel per strip) that gives an OR output; they are 200 such cards. A central unit provides different OR levels, still allowing the separate readout of its input channels.

The gas system is monitorized in such a way as to switch off automatically the high voltage if the percentages of Argon and Butane change outside given limits.

## 6. Other measurements

Other reactions, besides the ones needed for monitoring purposes, can be studied with a $\overline{n}n$ dedicated apparatus. We report on them shortly, just to give an idea of physical potentialities; more detailed calculations and simulations are foreseen. In all cases the central tracking detector plays an essential role. The related triggers are discussed separately in section 6.5.

### 6.1 Strange baryon form factors

These form factors have never been measured either in the time-like or in the space-like region. Ref. 3, which is in good agreement with known proton form factor measurements, predicts that reactions

$$e^+e^- \rightarrow \Sigma^+ \overline{\Sigma}^+ \ , \ e^+e^- \rightarrow \Sigma^- \overline{\Sigma}^-$$

have the largest cross sections among strange baryon production, of the order of 0.1nb near threshold ($\sqrt{s}$=2.379 GeV and 2.395 GeV respectively). We can look at the final state $\overline{n}n\pi^+\pi^-$ (branching ratio 25% with $\Sigma^+\overline{\Sigma}^-$ and 100% with $\Sigma^-\overline{\Sigma}^+$). Measurements of pions and $\overline{n}$ directions and of $\overline{n}$ energy by TOF are in principle sufficient to recognize the reaction kinematically, using the constraints on $\Sigma$ masses. Further checks come from the projected origins of the pion tracks that must be outside the beam ($c_\tau$ is 2.4cm for $\Sigma^+$ and 4.4cm for $\Sigma^-$). Of course the events are more constrained in case of neutron detection.

### 6.2 Total multihadron cross section

In fig. 17 we show a weighted mean, taking into account statistical errors only, of the multihadron cross section available up to now in the Adone energy range. The $\sqrt{s}$ interval 1.4-2.4 GeV has been estensively studied by DM2 and the results are expected soon; in the interval 2.4-3.0 GeV the cross section measurements are very poor.

The not flat behaviour above 2 GeV used to be explained with an increasing contribution of
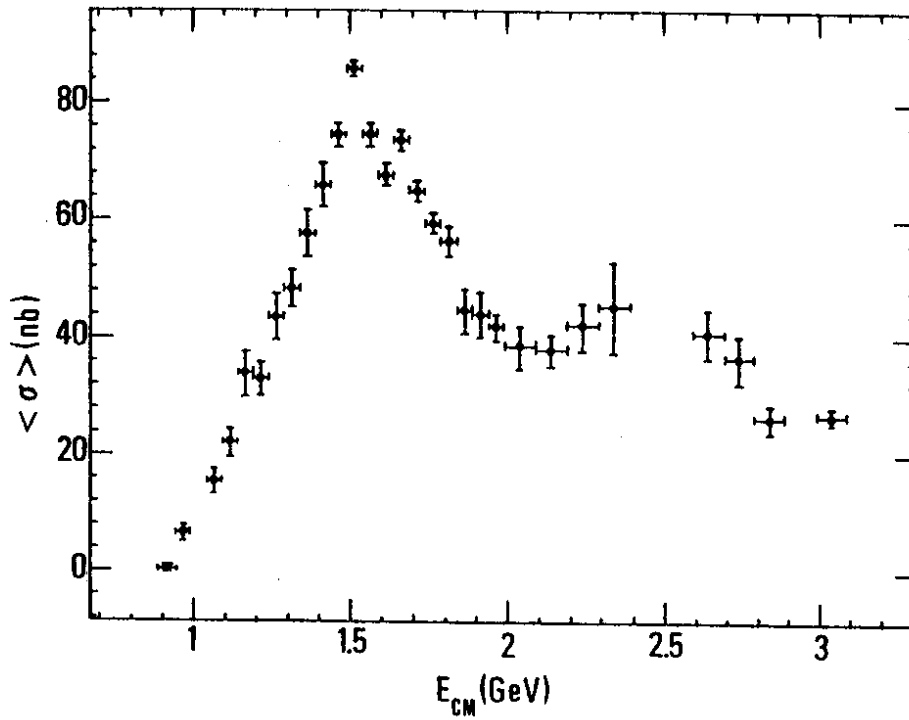
channels with strange particles, but



*fig.17*

inclusive $K_s^\circ$ production studies done by DM1[17] up to 2.2 GeV do not agree with this explanation (see fig. 18). Clearly a detailed measurement of
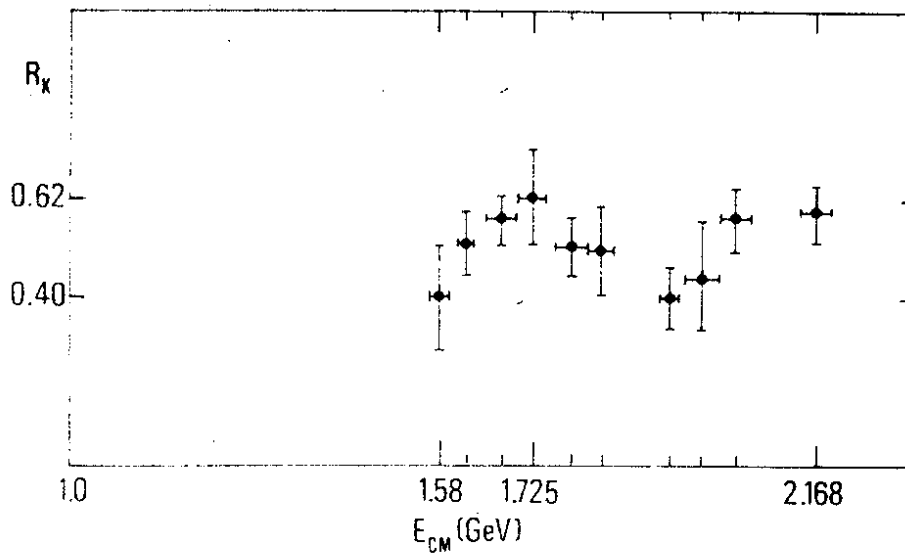


*fig.18*

total cross section from 2 to 3 GeV would be very interesting. Some characteristics of our set-up, as large solid angle, low trigger threshold and short interaction length, make it suitable for such a measurement. This is true also for contributions to total cross section coming from reactions with Kaons, which are delicate to evaluate in a non magnetic detector; $K_s^\circ$ can be partially identified with the expected vertex reconstruction accuracy ($c_\tau = 2.7$cm) and $K_L^\circ$ can convert in the iron absorbers.

## 6.3 J/Ψ physics

A few days of measurements at 3.1 GeV should allow a good determination of the branching ratio B(J/Ψ→n$\overline{n}$); the only published data[18] give B=(0.18±0.09).

At this higher energy $\overline{n}$ and $n$ have each 0.61 GeV of kinetic energy, i.e. p=1.23 GeV/c, β=0.795; consequently the TOF discrimination can be marginal in some cases and it is safer to impose also neutron detection. Still one can expect to detect ≈15$\overline{n}n$ events per day.

A large difference between $\overline{p}p$ and $\overline{n}n$ branching ratioes can arise from electro-magnetic contributions in the J/Ψ coupling to $\overline{n}n$ with respect to the simple isospin prediction of equal branching ratioes. A good knowledge of this coupling is requested, for instance, in the prediction of the proton lifetime.

Another major point of interest is related to the discovery by Mark III at SPEAR[19] of a resonance ( ξ(2230) ) in the $K\overline{K}$ mass at M= 2230MeV, whose width $\Gamma = 26\,^{+20}_{-16} \pm 17$ MeV is compatible with zero once the mass resolution has been taken into account.

The ξ has been discovered and confirmed in two subsequent runs, 3 millions of hadronic events each, studying (see fig. 19)

$$J/\Psi \to \gamma K^+ K^- \qquad , \qquad J/\Psi \to K_s^\circ K_s^\circ$$

But this risonance is still controversial. The DM2 experiment at the Orsay DCI[20] had no evidence in a total of 8 million hadronic events (see fig.20). Searches for a direct production in $\overline{p}p \to K^+K^-$ have given negative result[21,22].

fig.19

$$J/\Psi \rightarrow \gamma K^+ K^-$$

events/15 MeV

$K^+K^-$ mass (GeV$^2$)

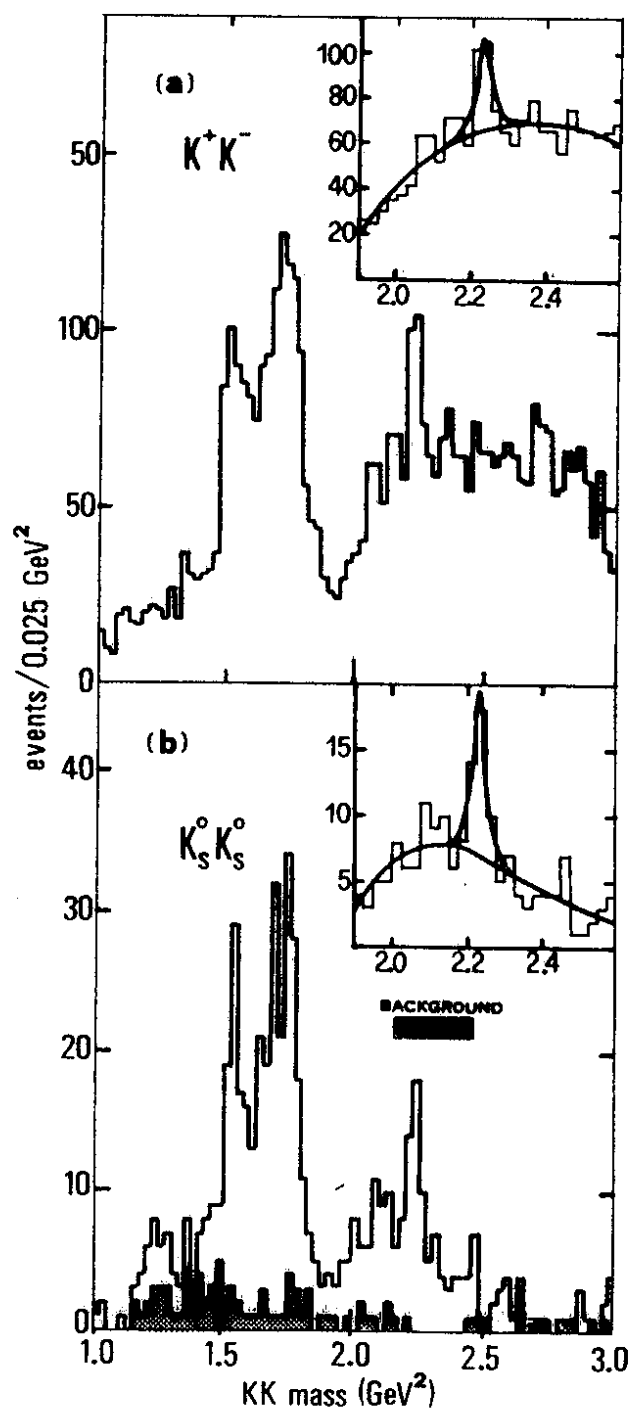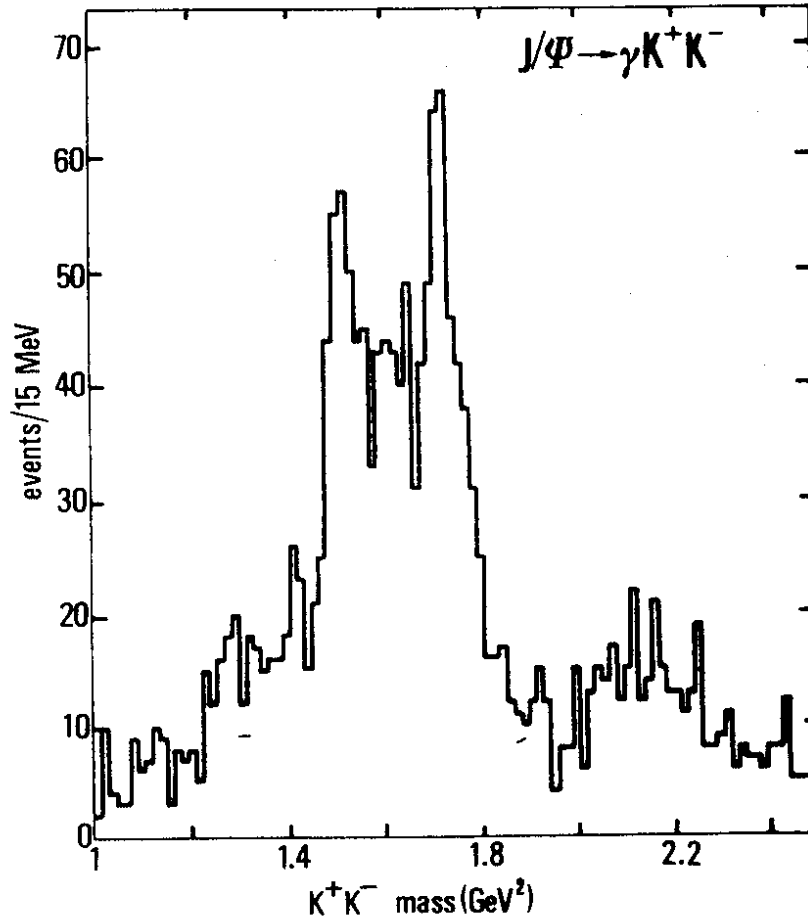*fig. 20*

The $\xi$ interpretation, if this state exists, is not unambiguous. In case of spin zero the only plausible possibility is a Higgs boson[23], in spite of the unspected mass. If the spin is 2 the $\xi$ could be interpreted as a $s\bar{s}$ $2^{++}$ excited state[24]. However for the first time an excited state would have a width narrower than the ground level, $f'(1925)$, whose width is 70 MeV.

There is no storage ring, but ADONE, that will operate at the J/$\Psi$ in next future. The espected J/$\Psi$ counting rate at ADONE is the same which was obtained at SPEAR, ~1 hadronic event per second, taking into account different luminosities and energy resolutions. Therefore a total of ~4 million events, necessary to test the $\xi$ esistence, can be obtained in a few month run.

The FENICE experiment can contribute, according to a preliminary analysis, studying the decays

$$J/\Psi \rightarrow \gamma K^\circ_L K^\circ_L \qquad , \qquad J/\Psi \rightarrow \gamma K^+ K^-$$

The neutral channel can be identified, in principle, due to the iron absorbers which allow neutral hadrons detection. Once three points are identified ($K^\circ_L$ interaction points, assumed measured within ~2 cm, and $\gamma$ conversion point, assumed measured within ~1 cm) the full event kinematics can be exploited; the beam interaction point is given by the intersection of the beam line with the plane defined by the three afovementioned points. A $\pm 20$ MeV resolution in the $K^\circ_L K^\circ_L$ invariant mass can be achieved, with suitable cuts on the experimental sample.

In fig. 21 the Mark III $K^\circ_s K^\circ_s$ mass spectrum is reported as detected by FENICE, according to a Montecarlo simulation. The overall detection efficency is ~35%.
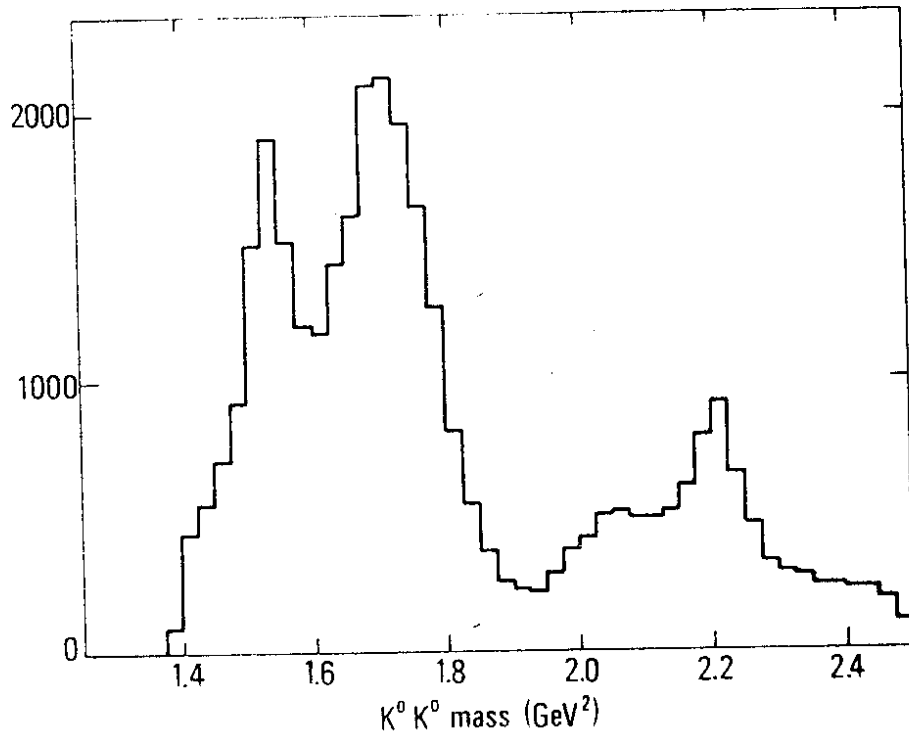


*fig. 21*

Background events, that could come from $J/\Psi \rightarrow 3\gamma$ and $J/\Psi \rightarrow \gamma n \bar{n}$, appear as negligible contributions, at least at this stage of the analysis.

The charged channel $\gamma k^+ k^-$ should be fully identified also in a non magnetic detector like FENICE once the apparatus is upgraded by an aerogel Cerenkov counter , able to distinguish with good efficency charged particles in the region of interest, as shown in fig. 22. Indeed a preliminary

study of DM2 events has demonstrated that the only processes contributing to 2 charged prongs + 1 hard photon coplanar events are the genuine 3 body decays

$$J/\Psi \; \rightarrow \; \gamma(\pi^\circ) e^+ e^- \quad , \quad \gamma(\pi^\circ)\pi^+\pi^- \quad , \quad \gamma(\pi^\circ) k^+ k^- \quad , \quad \gamma(\pi^\circ)\bar{p}p$$

However, the $\beta$ spectra do not overlap, if anomalous geometrical configurations are not considered.



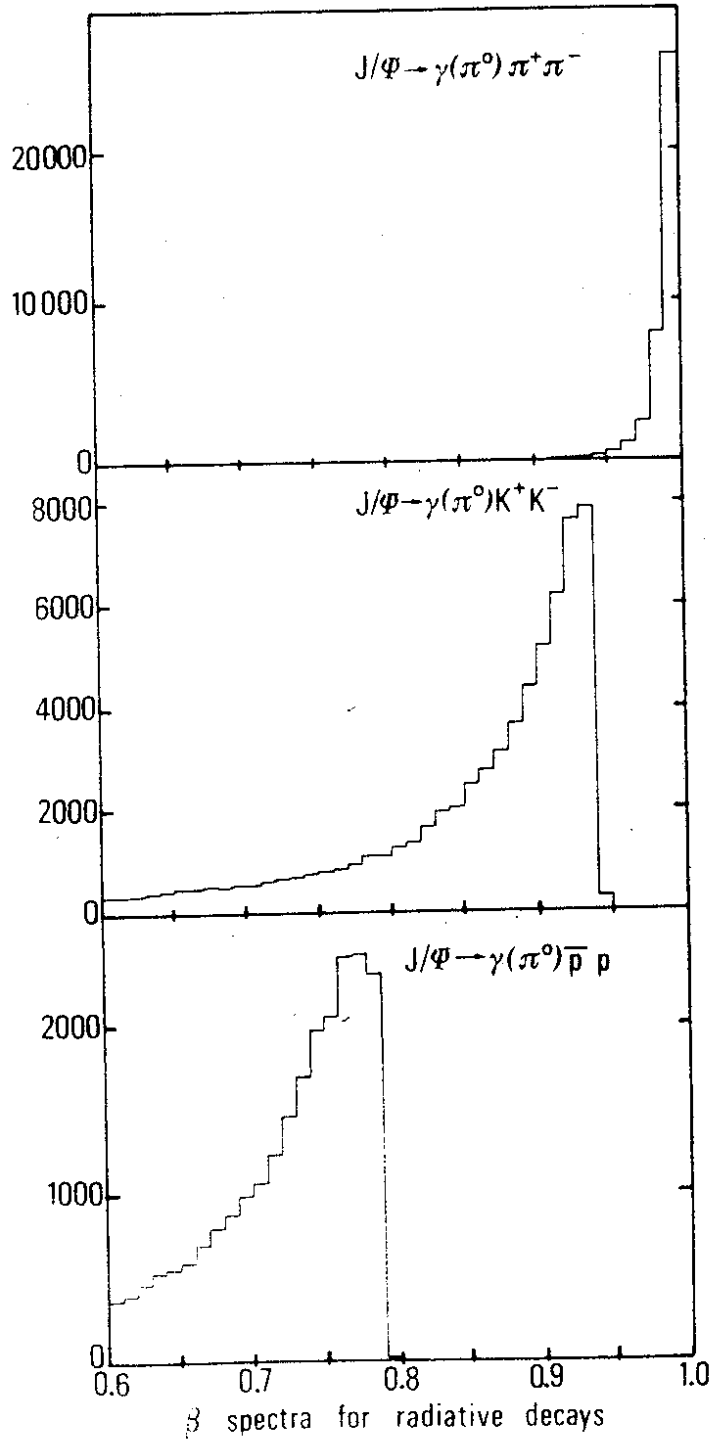$\beta$ spectra for radiative decays

fig 22

The experimental feasibility of all these hypotheses will be partially tested in the first runs at the $J/\Psi$.

## 6.4 Monitor reactions

The reference reactions for an absolute determination of the $\overline{n}n$ cross section can be $e^+e^- \to e^+e^-$ and $e^+e^- \to \mu^+\mu^-$ (see section 3.4) and we plan to measure them in parallel with the main reaction.

A different monitor is $e^+e^- \to \overline{p}p$; it would be important to have at least one measurement overlapping the DM2 ones, that go up to $\sqrt{s}=2.2$ GeV, and then to collect data in this channel at all other higher energies. The main difficulty is the short range of the proton; however, already at $\sqrt{s}=2$ GeV it should reach the first layer of neutron counters.

## 6.5 Related triggers.

The above reactions need a corresponding trigger and indeed some of them are already foreseen in the scheme of section 4.5.

A common denominator is the "one charged track" trigger that requires the coincidence of three counters in three different planes with a pointing geometry; suitable combinations of this trigger generate the $e^+e^-$ and $\mu^+\mu^-$ (in general a collinear two body trigger) and the multihadron trigger, where at least three tracks are required. In all these cases the veto hodoscope around the pipe is used in coincidence. A problem in the $\mu^+\mu^-$ trigger is given by the cosmic ray veto that has to be released for this trigger since the muons are not stopped by the concrete shield.

The other triggers are at present under study. For the $\overline{p}p$ trigger it should be sufficient to ask for a coincidence between the veto hodoscope and the first layer of neutron counters ($\overline{p}$ signature) and a similar coincidence with more hits in the opposite direction ($p$ signature). Again a coincidence between antineutron and neutron signature is necessary at the $J/\Psi$. For the strange baryon production we have first to simulate it in our apparatus in order to find a trigger configuration.

## 7. Plans for the experiment

In this conclusive section we want to summarize the needs for beam time and data taking plans.

The expected trigger rate is $\leq 10$ s$^{-1}$ and is due essentially to fake cosmic ray triggers. This calls on one side for an efficient filter procedure before writing on tape; on the other side one can profit of these triggers for calibration purposes.

The expected numbers of events per second with a luminosity of $3 \cdot 10^{29}$ cm$^{-2}$s$^{-1}$ are:

| final state | $\sqrt{s}$=1.95 GeV | $\sqrt{s}$=2.45 GeV |
|---|---|---|
| $\overline{n}n$ | $1.0 \cdot 10^{-4}$ | $2 \cdot 10^{-5}$ |
| $(\overline{n}n)$ | $1.7 \cdot 10^{-5}$ | $3.5 \cdot 10^{-6}$ |
| $e^+e^-$ | $6 \cdot 10^{-2}$ | $5 \cdot 10^{-2}$ |
| $\mu^+\mu^-$ | $4 \cdot 10^{-3}$ | $3.5 \cdot 10^{-3}$ |
| $\overline{p}p$ | - | $3 \cdot 10^{-5}$ |
| $\overline{\Sigma}\Sigma$ | - | $2 \cdot 10^{-5}$ |
| multihadron | $8 \cdot 10^{-3}$ | $9 \cdot 10^{-3}$ |

These numbers include a rough estimation of acceptance and efficiency factors.
In a typical day of $8 \cdot 10^4$s we expect the following events:

| | | |
|---|---|---|
| $\overline{n}n$ | 8 | 1.6 |
| $(\overline{n}n)$ | 1.4 | 0.3 |
| $e^+e^-$ | 4800 | 4000 |
| $\mu^+\mu^-$ | 320 | 280 |
| $\overline{p}p$ | - | 2.4 |
| $\overline{\Sigma}\Sigma$ | - | 1.6 |
| multihadron | 640 | 720 |

(at 1.95 and 2.45 GeV respectively).

We plan to collect data for about one month at $\sqrt{s}$=1.95 GeV and for another month at $\sqrt{s}$=2.45 GeV; in the first case we can determine the form factor of the neutron near threshold with a statistical accuracy of $\approx 7\%$, in the second the error is $\approx 15\%$ for $\overline{n}n$ and $\approx 11\%$ for $\overline{p}p$; at the same level one should have also the $\overline{\Sigma}\Sigma$ channel. Besides these two points at least two more are foreseen, one around 2.2 GeV and the other around 2.7 GeV, with the same amount of running time as for the previous points. At the J/$\Psi$ we plan to take data for two weeks quite at the beginning in order to benefit of a faster calibration of the apparatus; later on we need two more weeks with the aim of a measurement of the branching ratio into $\overline{n}n$ and $\overline{p}p$ with a 10% error and a few month running time in case of a $\xi$ search.

It is however difficult to establish now a schedule; while the points near threshold (1.95 GeV), above $\overline{\Sigma}\Sigma$ threshold and at the J/$\Psi$ can be considered as fixed, it could be more interesting a scanning of the 2-3 GeV region aiming at a good determination of R and a less precise form factor measurement. A major unknown is the luminosity value; should it reach a value above $5 \cdot 10^{29}$ cm$^{-2}$s$^{-1}$, energy scanning and good statistical level for any reaction would become more compatible.

## REFERENCES

1. N.Cabibbo and R.Gatto, PR 124 (1961) 1577.
2. A.Zichichi et al., NC24 (1962) 170.
3. G.Korner and M.Kuroda, PRD16 (1977) 2165.
4. J.T.Seeman, "Beam-beam interaction: luminosity, tails and noise", Int. Acceler. Conf., Fermilab 1983.
5. F.Amman et al., "Remarks on two beam behaviour of the 1.5 GeV e$^+$e$^-$ storage ring Adone", Int. Acceler. Conf., Geneva 1971.
6. M.E.Biagini and M.Preger, Adone Int. Memo G-55, 1984.
7. S.Tazzari, "Beam-beam effects at the 1.5 GeV e$^+$e$^-$ storage ring Adone", AIP Conf. Proc. Brookhaven 1979.
8. S.Tazzari, Adone Int. Memo T-93.
9. H.C.Dehne et al., NIM 116 (1974) 345.
10. T.Bressani et al., IEEE Trans. on N.S. 32 (1985) 733.
11. G.Battistoni et al., NIM 164 (1979) 57.
12. P.Macciotta et al., IEEE Trans. on N.S. 33 (1985)
13. R.E.Marshak, Meson Physics, pg. 231-235, McGraw-Hill (1952)
14. M.Tavani and D.Zanello, Int. note 805 (1983), Dep. of Physics, 1$^{st}$ Rome Univ.
15. F.Ashton et al., J.Phys. A4 (1971) 352.
16. R.Santonico and R.Cardarelli, NIM 187 (1981) 377.
17. B.Delcourt et al., Proceedings of the 1981 Intern. Symp. on Lepton and Photon Interactions at high energies, Bonn 1981, pg. 205.
18. H.J.Besch et al., PL 78 (1978) 347.
19. R.M. Baltrusaitus et al., PRL 56 (1986) 107.
20. J.E. Augustin et al., LAL 85/27, July 1985 and Berkeley Conference 1986.
21. J.H. Christenson et al., Berkeley Conference 1986.
22. PS 170 experiment at CERN, submitted to PLB.
23. H.E. Haber and G.L. Kane, PL 135 B (1984) 196,
    R.M. Barnett et al., PR D 30 (1984) 1529.
24. S. Godfrey et al., PL 141 B (1984) 439.